Evidences for strong directional resonances in intensely deformed zones of the Pernicana fault, Mt. Etna (Italy)

Di Giulio G.[1], F. Cara[1], A. Rovelli[1], G. Lombardo[2], and R. Rigano[2]

1) *Istituto Nazionale di Geofisica e Vulcanologia, Via di Vigna Murata 605, 00143 Rome, Italy*
2) *Dipartimento di Scienze Geologiche, Università di Catania, Corso Italia 55, 95129 Catania, Italy*

Abstract

In this paper we investigate ground motion properties in the western part of the Pernicana fault. This is the major fault of Mt. Etna and drives the dynamic evolution of the area. In a previous work, *Rigano et al.* [2008] showed that a significant horizontal polarization characterizes ground motion in fault zones of Mt. Etna, both during earthquakes and ambient vibrations. We have performed denser microtremor measurements in the NE Rift segment and in intensely deformed zones of the Pernicana fault at *Piano Pernicana*. This study includes mapping of azimuth-dependent horizontal-to-vertical spectral ratios along and across the fault, frequency-wavenumber techniques applied to array data to investigate the nature of ambient vibrations, and polarization analysis through the conventional covariance matrix method. Our results indicate that microtremors are likely composed of volcanic tremor. Spectral ratios show strong directional resonances of horizontal components around 1 Hz when measurements enter the most damaged part of the fault zone. Their polarization directions show an abrupt change, by 20° to 40°, at close measurements between the northern and southern part of the fault zone. Recordings of local earthquakes at one site in the fault zone confirm the occurrence of polarization with the same angle found using volcanic tremor. We have also found that the directional effect is not time-dependent, at least at a seasonal scale. This observation and the similar behaviour of volcanic tremors and earthquake-induced ground motions suggest that horizontal polarization is the effect of local fault properties. However, the 1-Hz resonant frequency cannot be reproduced using the 1-D vertically varying model inferred from the array data analysis, suggesting a role of lateral variations of the fault zone. Although the actual cause of polarization is unknown, a role of stress-induced anisotropy and micro-fracture orientation in the near-surface lavas of the Pernicana fault can be hypothesized consistently with the sharp rotation of the polarization angle within the damaged fault zone.

1. Introduction

The Mt. Etna Volcano is located in a complex tectonic region at the boundary between African and European Plates [*Barberi et al.*, 1974; *Lentini*, 1982]. Mt. Etna, more than 3300 m high and with a diameter of about 40 km, is a basaltic stratovolcano characterized by eruptive and explosive behaviour. Tectonic activity in the area produced extensional fractures, faults and grabens well-evident along the unstable NE flank [*Billi et al.*, 2003; *Tibaldi and Groppelli*, 2002]. In particular, the active Pernicana fault system (*PFS* hereinafter) is one of the most significant tectonic structures of the NE flank. It is a roughly EW oriented strike-slip fault (Fig. 1) with a length of about 18 km from the NE rift to the Ionian coastline [*Neri et al.*, 2004]. The western part of the *PFS* is the most active of the flank faults and corresponds to the northern margin of the instability that affects the SE flank of the volcanic edifice [*Rust et al.*, 2005]. In the last decades, the central portion of the *PFS* has been characterized by creep processes with displacement of about 2 cm/year [*Azzaro et al.*, 2001; *Obrizzo et al.*, 2001]. The *PFS* was reactivated during the recent 2002-2003 eruption in the nearby NE Rift [*Acocella and Neri*, 2005; see Fig. 1]. Active volcanic faults as the *PFS* are usually characterized by closely-spaced fractured rocks and represent a natural laboratory as being likely preferential pathways for fluid migration. Therefore gas soil emission has been frequently monitored along the main structures of Mt. Etna including the *PFS* [e.g. *Immè et al.*, 2006a and 2006b; *Morelli et al.*, 2006; *Brogna et al.*, 2007; *Burton et al.*, 2004]. Also volcanic tremor can shed light on the physical processes of the volcano. Many studies indeed deal with the volcanic tremor wave-field on Mt. Etna trying to identify microtremor properties during either quiescent or eruptive periods [*Gresta et al.*, 1987; *Ferrucci et al.*, 1990; *Del Pezzo et al.*, 1993; *Ereditato and Luongo*, 1994; *Wegler and Seidl*, 1997; *Ripepe et al.*, 2001; *Privitera et al.*, 2003; *Saccorotti et al*., 2004]. Changes in time and space of background seismic noise related to the volcanic activity are well documented. *Falsaperla et al.* [2005] showed remarkable variation in amplitude and frequency content of the tremor of Mt. Etna at seismic stations surrounding the summit crater area before and during the volcanic activity of July-August 2001. During the 2001 flank eruption they observed high tremor amplitude and a shift of the predominant frequencies towards frequencies (about 2 Hz) lower than those of the pre-effusive phase. Based on the amplitude decay of seismic stations they also found a source migration from a depth of about 5 km towards the first half kilometer from the surface. *Bianco et al.* [2006] studied local earthquakes of the 2001 volcanic eruption finding changes of shear wave splitting parameters preceding the main eruptive phenomena. The temporal changes of shear wave splitting parameters are interpreted in terms of variations of local stress field at Mt. Etna acting at the upper crust. Similarly to *Falsaperla et al.* [2005], the technique of amplitude decay versus distance using permanent stations near the crater area was also adopted from *Di Grazia et al.* [2006]. They analyzed tremor data during the September 2004 lava effusion through a 3D grid search localizing the tremor source in a region close and partially overlapped to the summit craters (SUM in the lower panel of Fig. 1). Their study also observed a migration of the source locations towards the south from the pre-eruptive phase to the lava effusion period. Using data from two dense small-aperture array of seismometers, *Di Lieto et al.* [2007] identified two tremor sources of the 2004 eruption of Mt. Etna located beneath the southeast crater (SEC in the lower panel of Fig. 1) and near the eruptive fissures of the eastern flank.

Interestingly, tremor data at different volcanoes outline energy mainly at long period showing similarity with low-frequency earthquakes typical of volcanic areas [*Fehler*, 1983; *Chouet*, 1985 and 1996; *Jousset and Douglas*, 2007; *Milana et al.*, 2008]. Despite the properties of volcanic tremor being non-unique and differing from one volcano to another, the most reliable tremor source mechanism seems to involve interaction between magmatic fluids within the surrounding fluid-filled cracks [*Seidl et al.,* 1981; *Konstantinou and Schlindwein*, 2002].

The goal of this paper is to study ground motion properties of the *PFS* focusing on the *Piano Pernicana* area (see Fig. 1). We deployed small-scale arrays (aperture of about 100 m) at *Piano Pernicana* to investigate the origin and dispersive nature of ambient vibrations. Coherent waves coming from the crater area were discerned, suggesting ambient vibrations are mostly composed of volcanic tremor. Array data also provided a dispersion curve estimated through the frequency-wavenumber (*f-k*) technique, leading to a one-dimensional (1D) shear-velocity profile. Additionally we performed 48 microtremor measurements; these data were analysed in terms of horizontal-to-vertical spectral ratios and polarization. In particular, we studied the western part of the *PFS* (at *Piano Pernicana*) along two parallel profiles crossing the fault zone, and the area close to NE Rift (Fig. 1). In the most damaged portion of *PFS*, results show strong directional amplification in the horizontal components of volcanic tremor. Tentative hypotheses for the explanation of the strong directional effects have been formulated.

2. Array experiments, tremor measurements, and analysis methods

We analyzed seismic data collected on Mt. Etna combining different methodologies and instruments. First, we recorded data from small-aperture arrays deployed in the westernmost part of *PFS* (*Piano Pernicana)*, about 1450 m above sea level (Figs.1 and 2). In the *Piano Pernicana* area, the 2002-2003 Etna activity caused significant surface fracturing on walls and paved and unpaved roads with a left-lateral displacement of more than 1.25 m in early November 2002 (the strong road deformation is shown in Fig. 3 of the paper by *Acocella and Neri*, 2005). We adopted both linear and 2D geometry for the array experiments, about 100 m north of the main trace of the Pernicana fault (see the lower panel of Fig. 2). In the linear array arrangement, we employed standard vertical geophones and a multi-channel recording-system commonly used in near-surface studies. In the 2D configuration we employed seismological stations equipped with data-logger connected to three-components seismometers. Further data consist of ambient noise measurements at different sites of Mt. Etna recorded by seismological stations (see Table 1 and black circles of Fig. 2) over a brief period of time (about 30 minutes). Tremor measurements were mostly localized around the array area at *Piano Pernicana*; several measurements were also performed in the portion of the *PFS* closest to the crater area, near the NE Rift (Fig. 2). *Di Grazia et al.* [2006] put the centroid of the tremor source during the September 2004 activity about 5 km south-west of the NE Rift. In the following we proceed by describing the experimental set-up, data collection procedures and analysis methods.

In October 2006 we deployed two small-aperture linear arrays of geophones. The first one was elongated in an approximately EW direction, and the other was orthogonal. The mid-points of the two arrays were coincident. The two linear arrays were equipped with 4.5 Hz vertical geophones that recorded active signals induced by a mini-gun source, with a sampling rate of 0.25 milliseconds (Fig. 3). Time length of each individual recording was 16.384 s. We used the Geometrics Geode system as multi-channel data logger. Each linear array was composed of 48 vertical geophones equally spaced at 2 m with a maximum length of 94 m. Seven shots using the mini-gun source were carried out along each line with a maximum offset of 20 m. Fig. 3 shows an example of shot recordings.

Along the same lines as the two linear arrays of geophones, we also deployed a 2D array composed of 16 seismological seismometers in a cross-shape configuration (Fig. 4). The seismological seismometers are three-component velocity transducers (Lennartz LE-3D/5s) with eigenfrequency of 0.2 Hz. This 2D array recorded volcanic tremor for about half-hour of the October 11, 2006. Each seismometer was connected to a Reftek 130-01 or a Lennartz MarsLite digitizer (24-bit and 20-bit A/D converter, respectively) and the sampling rate was of 125 Hz. Since in the frequency band of interest the instrument response is flat in velocity, we did not deconvolve the records by the instrument transfer function. The absolute timing was provided by a GPS receiver connected to each digitizer.

Active data recorded by the two linear arrays of geophones have been processed by applying standard array techniques commonly adopted in engineering-geotechnical practice [*Rickwalski et al.*, 2007]. These techniques are based on multi-channel analysis of surface waves (MASW) [*Park et al.*, 1999; *Louie,* 2001]. The 2D geometry and the use of long-period seismological sensors permit estimates of source back-azimuth of volcanic tremor through *f-k* analysis [*Kvaerna and Ringhdal*, 1986]. The inversion of the combined dispersion curves, inferred from the geophone linear arrays and the 2D seismometer array, allows the evaluation of a shallow 1D velocity profile. The inversion procedure is based on a neighbourhood algorithm [*Sambridge*, 1999] as implemented by *Wathelet* [2005].

In addition to the array experiments, we performed just over 30 measurements of volcanic tremor through mobile stations on the north-eastern flank of Mt. Etna during five different surveys in May and October 2007, and April, June, and November 2008. Measurements were concentrated in proximity to the main fault trace at *Piano Pernicana,* including studying the tremor properties along two approximately parallel transects (about 900 m apart) (lower panel of Fig. 2). Table 1 lists the positions and times of these measurements of volcanic tremor. Each measurement consists of about half-hour time series (see Fig. 5 for examples of data), using Reftek 130-01 data-loggers and Lennartz LE-3D/5s three-components sensors, with a sampling rate of 125 Hz.

In order to identify site-specific directional effects, tremor data are analyzed using two complementary methods. First, we use the conventional method for the determination of the polarization direction, based on eigen-decomposition of the covariance matrix of the three components of ground motion [*Kanasewich*, 1981; *Jurkevics*, 1988]. We adopt the procedure implemented by *La Rocca et al.* [2004] plotting the azimuth of polarization vector on the horizontal plane as rose diagram. The conventional covariance matrix method is applied to data after band-pass filtering in the frequency band 0.4-6 Hz. Second, we compute the horizontal-to-vertical spectral ratio (HVSR) as a function of the frequency and direction of motion as introduced by *Spudich et al.* [1996] and successively exploited by *Cultrera et al.* [2003] and *Rigano et al.* [2008]. The horizontal plane is divided into a set of directions uniformly spaced at intervals of 10°, from 0° (north) to 180° (south). HVSR for the 18 rotated horizontal components is computed searching for azimuthal variations. The azimuth-pattern of HVSR complements the rose diagrams giving i) clear indication of the frequencies where directional effects occurs, and ii) the level of horizontal ground motion compared to the vertical one. As found by *Rigano et al.* [2008] at Mt. Etna, the directions inferred from the azimuth-pattern of HVSR are consistent with those provided by the covariance matrix method.

3. Results

3.1 H/V spectral ratios and polarization

The time-histories and the Fourier amplitude spectra shown in Fig. 5 are representative of tremor measurements carried out along the NE flank of volcano during the surveys of May and October 2007 (Table 1). The spectra of the horizontal components are characterized by much larger energy and complexity compared to the vertical component up to 2 Hz (Fig. 5). The east-west component of measurement sites #30 and #5 shows larger amplitude than the north-south one, whereas measurement site #10 shows the highest energy for the north-south component.

Fig. 6 displays the results of horizontal-to-vertical spectral ratios for the measurements of October 2007 survey in the *Piano Pernicana* area. The time-histories were first visually checked to exclude strong transient disturbances. This reduces the effective length by 20% to 50%. Therefore, the tremor data of the two horizontal components were rotated from 0° to 180°, and for each bin of the rotation angle were cut into 1-min long time-windows, detrended and processed with a 5% Hanning taper and with a fast Fourier transform algorithm. The resulting Fourier amplitude spectra were smoothed using a 0.1 Hz running frequency window. The

horizontal-to-vertical spectral ratios for each of the 1-min windows were geometrically averaged over the window ensemble. The geometric mean of HVSRs are represented in Figure 6 as contour plots where the x-, y- and z-axes are frequency, rotation angle and spectral ratio amplitude, respectively. HVSRs near the *PFS* show a strong directional effect around 1 Hz. Interestingly, a group of HVSRs in the southern part (#3, #4, #5 and #6 of Fig. 6) shows a predominant direction of about 120° (measured clockwise from geographic north) in the frequency range 0.7-2 Hz. The remaining measurements (#7, #9, #10, #11, #12, #13 and all of the stations of the 2D array), to the north-east of the first group, show a directional effect around 160° in the same frequency band (Fig. 6). Results of conventional covariance matrix analysis are also shown in Fig. 6 as rose diagrams. The polarization vector at each station was measured by diagonalizing the covariance matrix using the technique already adopted by *Rigano et al.* [2008]. It moves a time-window of 2 sec with a 50% partial overlap throughout the entire tremor record of each site (the same used for the computation of HVSR). In this way, about 600 to 2000 values of polarization are computed for each site and represented as rose diagrams. The histograms (Fig. 7) show unimodal trends clearly peaked at the mean value of 117° and 167° for measurements to south and north, respectively, of the fault trace. Their statistical uncertainties are ± 11° and ± 25°, respectively, thus indicating a spatial variation well beyond statistical errors.
The distribution of polarization in rose diagrams is very consistent with the direction found through HVSR (Fig. 6). This indicates that the results obtained from the HVSRs are not biased by possible spectral holes in the spectrum of the vertical component which is used as the denominator.

Tremors recorded at the 2D array stations show a directional effect consistent with nearby measurements around the array (Fig. 6). All of the 16 seismological stations of the 2D array indicate a very similar azimuth-pattern in the HVSRs with a polarization of about 160° occurring at two close frequencies near 1 Hz (Fig. 8 top). This is also shown in the bottom panel of Fig. 8, where we have plotted on the same scale the HVSRs of the rotated component of horizontal motion along 160° at the array stations.

It is important to remark that the 2D array was deployed in October 2006, about a year before the nearby tremor measurements. The consistency of the directional effects between stations of the 2D array and the later measurements suggests that the directional effects inferred through volcanic tremor does not show significant variations as a function of time, at least at a seasonal scale. This is also confirmed by the fairly stable pattern of the HVSRs at site #5 (the camping ground *Clan Ragazzi;* see Table 1) where we repeated tremor measurements in May 2007, October 2007 and November 2008. Observations at this site, which shows horizontal polarization at about 120°, indicate that November 2008 was characterized by a larger horizontal ground motion excitation around 1 Hz. This was probably due to the eruptive activity of this period, with tremor amplitudes at crater stations slightly larger than the previous periods (Susanna Falsaperla, personal communication). This is reflected in the larger peak of HVSRs (Fig. 9) in the November 2008 measurement. A part from this difference in a narrow frequency band, the pattern of the three periods is significantly similar.

The most significant directional effects at stations near the fault are observed at about 1 Hz. The particle motion at this frequency demonstrates how strong the polarization of volcanic tremor is in the horizontal plane (Fig. 10a). The ground motion in the vertical plane is substantially constant in amplitude, whereas the horizontal motion becomes progressively larger when measurements enter the fault zone. Our results show that the ground motion is amplified in preferential directions, which is the typical behaviour of directional resonances as defined by *Bonamassa and Vidale* [1991] and *Bonamassa et al.* [1991].

During the survey of April 2008 we intensified tremor measurements in the portion of the *PFS* shown in Fig. 6 where the change of horizontal polarization was observed. Fig. 11 shows the results of these new measurements. Both the HVSR patterns and the covariance matrix polarization analysis confirm the rotation, along this transect crossing the fault zone from south to north, at about 1 Hz from 120° to 160° (see #16, #17, #18 and #19 of Fig. 11). This change of direction is very abrupt occurring over a distance of 50 m between adjacent measurements (#17 and #19 of Fig. 11). In April 2008 we also investigated a different area of the *PFS* at *Piano Pernicana*. We collected tremor about 900 m to the east of the previous measurements (#20 to #28, see Fig. 11). The results of this new transect also show a strong horizontal polarization around 1 Hz, with an amplitude of the HVSR peaks that seems to decrease as a function of the distance from the fault scarp (Figs. 10b and 11). The rotation of polarization around 1 Hz north of the *PFS*, although still present, is less evident compared to some of the previous results of the western transect (comparing Fig. 11 with Fig. 6; see also Fig. 10b). HVSRs also indicate an increase of the resonance peak from 1 Hz to 1.3 Hz moving to the north.

Single-station measurements were also performed up to 5 km from the array site (Fig. 12), including the portion of the *PFS* closest to the crater area, near the NE Rift. Fig. 12 shows the HVSR and the polarization results. A different behaviour of volcanic tremor emerges clearly within the area close to the crater (#29, #30 and #31, elevation between 2000 and 2400 m above sea level) and at other sites 1 to 5 km from the fault trace (#1, #2, #8, #14 and #32). Measurements #29, #30 and #31 show spectral peaks of tremor in the frequency band up to 2 Hz with a predominant polarization of about 90° (Fig. 12). In detail, measurement #29 at the highest elevation shows HVSR with different narrow peaks. The HVSR amplitude is about 5 at 0.6, 0.9, and 1.8 Hz, whereas it is a factor of 8 at 1.3 Hz. The two adjacent measurements #30 and #31 show a consistent spectral peak only below 1 Hz and the polarization is also roughly east-west (Fig. 12). In contrast, the remaining measurements of Fig. 12 indicate a predominant north-south polarization, although they do not show clear spectral peaks since the HVSR is almost flat (maximum amplitude below 2). Note that measurement #2, which is the nearest the array site of *Piano Pernicana,* shows similar spectral properties to the array area: i.e., the HVSR peak at about 1 Hz and the 160° polarization (see Figs. 6, 8 and 11), although at a smaller level of HVSR amplitude (a peak amplitude of 4). It is also interesting that our finding of a predominant north-south polarization (excluding the sites near the NE rift) observed through tremor data is consistent with the fast polarization direction found by *Bianco et al.* [2007]. This author used shear-wave splitting analysis on local earthquakes recorded on the eastern flank of Mt. Etna by local seismic stations (see Fig. 12) considering different time periods including the 1989 and 2001 eruption.

3.2 Array data

Frequency-wavenumber (*f-k*) techniques have been applied to the array data collected at *Piano Pernicana* to derive the apparent slowness and back-azimuth of coherent wave trains. These techniques, generally used for surface waves analysis although they can be applied indifferently to body and surface travelling waves, pick the maxima of the *f-k* power spectrum estimator [*Tokimatsu*, 1997], allowing the reconstruction of propagation properties of the waves crossing the array.

The data processing of the two linear arrays was performed using two different *f-k* codes: the commercial software Remi [*Louie*, 2001] and the Geopsy program implemented in the framework of the research project Sesame (Site Effects Using Ambient Excitations, http://sesame-fp5.obs.ujf-grenoble.fr/index.htm). These two codes return consistent results and an example of the results of a shot is shown in Figure 13 (top panel). The linear arrays, which were equipped with vertical 4.5 Hz geophones and recorded active data, yield apparent slowness values in the 7-32 Hz frequency range. The final dispersion curve (Fig. 13 middle panel) also shows the slowness estimated in the 2-5 Hz frequency band through the 2D seismometer array using the vertical component of volcanic tremor. The dispersive character is clearly evident in Fig. 13, confirming our assumption of a predominant presence of surface Rayleigh waves in the vertical component of tremor. Furthermore, the 2D geometry of the array equipped with seismological sensors combined with the low-frequency content of volcanic tremor permit investigation of both i) lower frequencies compared to the linear geophone arrays and ii) propagation back-azimuths of travelling waves. The performance of an array configuration for deriving a dispersion curve depends on the array aperture and on the wave-field characteristics. According to the limits in terms of wavenumber, as explained in *Wathelet et al.* [2008], the resolution of our 2D array allows us to work with minimum frequencies of about 2 Hz, whereas above 5 Hz the array performance is biased by aliasing phenomena. Unfortunately, our array resolution is not able to resolve the 1 Hz frequency where we observe the most significant directional resonances. However, the directional effect peaked at 1 Hz is still persistent at 2 Hz (see Figs. 6 and 8).

The back-azimuth of the tremor wave-field inferred through the vertical components of the 2D array is stable around 220° in the frequency band 2-4.5 Hz (Fig. 13 lower panel). This direction points to the summit crater area (SUM of the lower panel of Fig. 1). In this case a single 2D array of limited aperture does not permit us to distinguish the possible presence of more than one tremor source, as found for Mt. Etna by *Saccorotti et al.* [2004] or by *Di Lieto et al.* [2007].

Finally we inverted the dispersion curve of Fig. 13 to obtain the 1D near-surface shear-velocity (v_s) profile of the site. The similar shape of HVSRs of the 16 array stations (Fig. 8, bottom panel) suggests that there are not strong lateral variations beneath the 2D array. The main assumption of the inversion procedure is that the vertical component of the tremor wave-field is predominantly composed of the fundamental mode of Rayleigh waves. The real nature of tremor wavefield is a complex mix of body and surface waves. However, a large contribute of fundamental mode Rayleigh waves to the dispersion characteristics of vertical component of motion is reasonable for low-frequency volcanic tremor [*Chouet et al.*, 1998; *Wegler and Seidl*, 1997].

Fig. 14 shows the 1D-layered velocity models using the neighbourhood algorithm [*Sambridge*, 1999] of the inversion procedure as implemented by *Wathelet* [2005]. The parameterization of the soil model was achieved using 3 main layers where we let the v_s increase with depth according to a power law. The power law exponent of each sediment layer, together with shear wave velocity and thickness, were free parameters during the inversion. The most superficial 2-m thick layer of inverted models is characterized by very low v_s (about 120 m/s) consistent with the presence of volcanic ashes and soft soil cover. The velocity gradient of the very shallow model, obtaining a maximum v_s of about 400 m/s at depth of about 25 m, reproduces fairly well the dispersion curve measured in the field (Fig. 14). The inverted velocity model at larger depth shows a stiff basement at about 30 m and v_s values in the range 1000-1400 m/s. This velocity is in agreement with velocity estimates inferred from previous arrays experiment of tremor data conducted by *Saccorotti et al.* [2004] on Mt. Etna.

In the inverted model, the combination of S-wave velocity and thickness of layers provides resonance frequencies that do not match the observed resonant frequency of about 1 Hz (Fig. 14 bottom). The lack of a 1-Hz peak in the theoretical transfer functions and the strong polarization of real data exclude an interpretation of the 1-Hz resonance simply in terms of laterally uniform isotropic site models.

4. Discussion

In a recent paper, *Rigano et al.* [2008] found that horizontal ground motion is polarized in fault zones of Mt. Etna. Microtremors as well as earthquakes at local and regional distances distinctly showed this feature in a fault zone of the south-eastern flank (namely the *TreMestieri* fault). They also found that polarization during earthquakes was independent of back-azimuth, depth and distance from the source. In this study, we focus our analysis on the *PFS* and find a similar conclusion for a site in the fault zone (#5 of Fig. 6, the camping ground *Clan Ragazzi* at *Piano Pernicana*) where we have collected both tremor and earthquake data. At site #5 a seismological station (Reftek130 coupled with LE-3D/5s) recorded continuously from 15 May 2007 to 29 May 2007. In this period the station registered two local and two regional earthquakes (Table 2) with satisfactory (≥ 3) signal-to-noise ratio in the frequency band of analysis. Fig. 15 shows the polarization angles of these earthquakes. The horizontal polarization of about 120° around 1 Hz at site #5, found through volcanic tremor (see Fig. 6), is confirmed well by waveforms of local and regional earthquakes (Fig. 15). Persistent polarization directions observed at site #5 using both noise and earthquakes with different epicentral distances and back-azimuths (Table 2) rule out a source effect and suggest the dependency of polarization on local properties of the site. Rectilinearity shown in Fig. 15 is also derived through the eigen-values of the covariance matrix [as defined in *Rigano et al.*, 2008]. It can assume values between 0 and 1 (spherical and rectilinear motion, respectively) and in general is used to discriminate between waves with different polarization properties. Fig. 15 shows that earthquake coda and noise are characterized by similar value of rectilinearity (about 0.85 on the average). This indicates an elliptical ground motion in good agreement with the particle motions of Fig. 10.

In general, damaged fault zones are characterized by reduced velocities and can trap seismic waves. This phenomenon is known as fault-guided waves and is responsible for a local amplification within the fault zone, as already investigated through theoretical models as well as observations [*Li and Leary*, 1990; *Rovelli et al.*, 2002; *Ben-Zion et al.*, 2003; *Lewis et al.*, 2005; *Wu et al.*, 2008; among many others]. In studies on fault-guided waves there is a large consensus in outlining that the amplitude of trapped waves tends to be maximum in the direction parallel to the fault strike. This does not occur in our study case: the observed polarizations of tremor are around 120° and 160° (see Fig. 6) whereas the Pernicana fault strike ranges from 70° to 98°. *Acocella and Neri* [2005] reported that the fault segments are mainly distributed at angles of 6° to 35° from the strike of the fault. Considering these values we can fit the 120° direction but not the 160° one. The same discrepancy between fault strike and polarization was also observed by *Rigano et al.* [2008] who, analyzing an abundant set of earthquakes recorded in the *TreMestieri* fault having a 135° strike, found a directional resonance with a NE-SW polarization. These authors excluded a role of guided waves generated in fault zone as responsible of directional resonance because the effect of polarization was persistent during the entire length of seismograms and not confined in dispersed phases after S-waves. Tentative computations using the few seismograms of Fig. 15 to get group-velocities at different frequencies lead to the same conclusion for the *PFS* as giving no evidence for dispersive guided waves. However experiments with denser collection of earthquakes in the fault zone would be needed to infer the nature of the incoming wave-field.

Rigano et al. [2008] also hypothesized that the preferred polarization of seismic signals could be related to anisotropy in the uppermost crust. As a matter of fact, the role of crustal velocity anisotropy on earthquake records of Mt. Etna has been already stressed by *Bianco et al.* [1996, 2006] and by *Bianco and Castellano* [1997]. These authors have conducted studies of shear-wave splitting and found evidences of an anisotropic volume with high-density cracks in the eastern slope of Mt. Etna with an estimated depth of 5 km. At a smaller scale, the important role of anisotropy along major faults, strictly depending on the local stress field of the shallow crust, is investigated in *Cochran et al.* [2003] and *Boness and Zoback* [2004]. It is worthy of note that *Cochran et al.* [2006], through earthquake data analysis, observed a spatial variation of fast shear-wave polarization around the San Andreas Fault at a distance range of about 100-400 m within the main fault trace. The stress-induced anisotropy of the Etnean rocks could cause aligned cracks in specific direction implying likely local changes of seismic velocities [*Schubnel and Guéguen*, 2003; *Becker et al.*, 2007], with the faster direction along the crack orientation. Faster velocity directions could imply lower attenuation directions resulting in polarized motions. Note that the occurrence of a differential amplification of the horizontal components does not affect the delay time between fast and slow components but only changes the final S-wave polarization after the delay-time correction. The results of *Bianco et al.* [2007] using shear-wave splitting of local earthquakes are consistent the predominant north-south polarization observed on tremor data on the eastern flank of Mt. Etna (see Fig. 12). Polarization could be an indicator of the stress field in the upper crust of Mt. Etna, and consequently of the anisotropic features of the medium.

The actual variation up to 40° of the polarization direction of the volcanic tremor observed at *Piano Pernicana* could be also consistent with the concept of stress rotation within fault zones. *Faulkner et al.* [2006] analyzed in detail the damage zone of a strike-slip fault in northern Chile using field observation, laboratory experiments and numerical modelling. Their study showed that the microfracture density varies as a function of distance from the fault causing variation of the elastic properties of rocks within the fault zone. Consequently a rotation of local stress can occur within the fractured damage zone of important faults.

At the present stage of the study, all our tentative interpretations of the origin of polarization in faults of Mt. Etna are purely speculative. Laboratory tests on rock samples and field experiments on velocity and attenuation variations as a function of azimuth are going on to check if anisotropy in fault zones is the right key of interpretation. We will also have the benefit of new multidisciplinary studies developed on Mt. Etna (including structural investigation of micro-and-macro fractures, fluid gas emission, seismicity as well as tremor properties) in the framework of the Project *V4-Flank* sponsored by the Civil Protection Department of Italy [*Puglisi and Acocella*, 2008].

5. Concluding remarks and perspectives

Sparse microtremor measurements and small-aperture seismic arrays deployed in intensely deformed zones provide polarization properties along the Pernicana fault system. According to *Rigano et al.* [2008], the azimuth-pattern of HVSRs of ambient vibrations complements conventional polarization analysis: the two techniques together appear a useful tool for recognizing directional effects in tectonically active areas of Mt. Etna. We have found that strong directional resonances of the horizontal components occur around 1 Hz near the NE Rift (Fig. 12) and at *Piano Pernicana* (Figs. 6, 8 and 11), where the largest deformations were observed during the 2002-2003 seismic activity. Measurements closest to the summit crater area show a nearly east-west polarization (Fig. 12) whereas at *Piano Pernicana* the directional resonances are characterized by an abrupt rotation of polarization (from 120° to 160°), occurring over distances as little as 50 m (Figs. 6 and 11).

Although the tremor properties are likely related to the activity of Mt. Etna, the directional effects evidenced at measurement sites in this study seem to be a local property and not time-dependent, at least on a seasonal scale during the investigated periods. Moreover, the predominant directions of polarization are common for tremor and earthquakes (Fig. 15). This is a strong indication that polarization can be affected by medium characteristics and local propagation properties. Caution is needed in interpreting polarization as a source feature only. Evidences of directional effects observed in highly deformed fault zones, if confirmed for the entire extension of the *PFS* and in other faults as well, could be a powerful tool to map highly deformed zones where urbanization or geological disturbances (e.g landslide, sedimentary deposits etc. etc.) mask the fault evidence at the surface. The next step of this study will be the continuation of microtremor measurements in the eastern part of the *PFS,* from *Piano Pernicana* up to the coast, to check the real feasibility of a mapping method using directional properties of ambient vibrations.

ACKNOWLEDGMENTS

We thank Giovanna Calderoni, Sebastiano D'Amico and Sergio Del Mese for their help in fieldwork during the experiment. We are grateful to John Haines, Francesca Bianco, Marco Neri, Marta Pischiutta, Francesco Salvini and Giuliano Milana for useful discussions. We also thank the Associate Editor, an anonymous and Martha Savage for very constructive reviews.

Table 1. Single station tremor measurements on the NE flank of Mt. Etna. Measurements #5, #16 and #33 were at different times at the same site (the camping ground *Clan Ragazzi*). The 16 sites of the 2D array are not listed (the array experiment was performed on October 11, 2006).

Date	**Start Time (UTC)**	**Lat (°)**	**Long (°)**	**Measur. number**
5 May 2007	09:03	37.7972	15.0268	#29
5 May 2007	09:48	37.7876	15.0110	#30
5 May 2007	10:37	37.7913	15.0178	#31
5 May 2007	17:00	37.7804	15.0528	#32
16 Oct 2007	09:33	37.8395	15.1164	#1
16 Oct 2007	10:42	37.8099	15.0881	#2
16 Oct 2007	13:12	37.8063	15.0669	#3
16 Oct 2007	13:41	37.8063	15.0673	#4
16 Oct 2007	14:09	37.8062	15.0675	#5
16 Oct 2007	14:40	37.8056	15.0668	#6
16 Oct 2007	15:21	37.8074	15.0683	#7
16 Oct 2007	16:10	37.8182	15.1011	#8
17 Oct 2007	09:45	37.8082	15.0730	#9
17 Oct 2007	10:21	37.8085	15.0715	#10
17 Oct 2007	10:52	37.8082	15.0699	#11
17 Oct 2007	13:12	37.8103	15.0652	#12
17 Oct 2007	13:47	37.8093	15.0661	#13
17 Oct 2007	14:38	37.8341	15.1099	#14
1 Apr 2008	12:08	37.8062	15.0675	#16
1 Apr 2008	11:48	37.8068	15.0680	#17
1 Apr 2008	13:04	37.8083	15.0692	#18
1 Apr 2008	13:18	37.8072	15.0675	#19
2 Apr 2008	09:46	37.8045	15.0786	#20
2 Apr 2008	09:58	37.8051	15.0787	#21
2 Apr 2008	10:48	37.8054	15.0790	#22
2 Apr 2008	10:48	37.8059	15.0794	#23
2 Apr 2008	13:15	37.8080	15.0763	#24
2 Apr 2008	13:33	37.8069	15.0789	#25
2 Apr 2008	14:22	37.8073	15.0786	#26
2 Apr 2008	15:07	37.8081	15.0796	#27
2 Apr 2008	15:21	37.8122	15.0804	#28
21 Nov 2008	15:21	37.8062	15.0675	#33

Table 2. Earthquakes shown in Fig. 15 and recorded at site #5 of Fig. 6 (the camping ground *Clan Ragazzi* at *Piano Pernicana*). The earthquake parameters are from the INGV seismological instrumental and parametric data-base (http://iside.rm.ingv.it/iside/standard/index.jsp).

Date	**Origin Time** (UTC)	**Lat.** **(°)**	**Long.** **(°)**	**Depth** (km)	**M**	**Epicentral dist. from site #5** (km)	**Backazimuth from site #5** **(°)**
15/05/2007	14:22:14	37.724	15.179	3	2.4	13	133
17/05/2007	05:48:13	38.571	14.687	19	3.6	91	339
21/05/2007	21:35:42	37.904	14.895	37	2.6	19	306
25/05/2007	09:39:46	39.658	16.834	10	3.9	257	362

References

Acocella, V., and M. Neri, Structural features of an active strike-slip fault on the slinding flank of Mt. Etna (Italy), *Journal of Structural Geology, 27*, 343-355, 2005.

Azzaro, R., M. Mattia, and G. Puglisi, Dynamics of fault creep and kinematics of the eastern segment of the Pernicana fault (Mt. Etna, Sicily) derived from geodetic observations and their tectonic significance, *Tectonophysics, 333(3-4)*, 401-415, 2001.

Barberi, F., L. Civetta, P. Gasparini, F. Innocenti, R. Scandone, and L. Villari, Evolution of a section of the Africa-Europe plate boundary: paleomagnetic and volcanological evidence from Sicily, *Earth. Planet. Sci. Lett., 22*, 123-132, 1974.

Becker, K., S. A. Shapiro, S. Stanchits, G. Dresen, and S. Vinciguerra, Stress induced elastic anisotropy of the Etnean basalt: Theoretical and laboratory examination, *Geophys. Res. Lett., 34*, L11307, doi:10.1029/2007GL030013, 2007.

Ben-Zion, Y., Z. Peng, D. Okaya, L. Seeber, L. G. Armbruster, N. Ozer, A. J. Michael, S. Baris, and M. Aktar, A shallow fault zone structure illuminated by trapped waves in the Karadere-Duzce branch of the North Anatolian Fault, western Turkey, *Geophys. J. Int.*, *152*, 699–717, doi:10.1046/j.1365-246X.2003.01870.x, 2003.

Bianco, F., M. Castellano, G. Milano, and G. Vilardo, Shear-wave polarization alignment on the eastern flank of Mt.Etna volcano (Sicily, Italy), *Annali di Geofisica, XXXIX*, 2, 429-443, 1996.

Bianco, F., and M. Castellano, The anisotropic volume of Mt. Etna: possible relationship with the stress-field, *Acta Vulcanologica, 9(1/2)*, 31-35, 1997.

Bianco, F., L. Scarfi, E. Del Pezzo, and D. Patanè, Shear wave splitting changes associated with the 2001 volcanic eruption on Mt Etna, *Geophys. J. Int., 167*, 959–967, doi: 10.1111/j.1365-246X.2006.03152.x, 2006.

Bianco, F., and L. Zaccarelli, A reappraisal of shear wave splitting parameters from Italian active volcanic area through a semiautomatic algorithm, *J. Seismol., 13(2)*, 253-266, doi: 10.1007/s10950-008-9125-z, 2007.

Billi, A., V. Acocella, R. Funiciello, G. Giordano, G. Lanzafame, and M. Neri, Mechanisms for ground-surface fracturing and incipient slope failure associated with the 2001 eruption of Mt. Etna, Italy: analysis of ephemeral data, *J. Volcanol. Geotherm. Res., 122*, 281-294, 2003.

Bonamassa, O., and J.E. Vidale, Directional site resonances observed from aftershocks of the 18 October 1989 Loma Prieta earthquake sequence, *Bull. Seism. Soc. Am., 81*, 1945-1958, 1991.

Bonamassa, O., J.E. Vidale, H. Houston, and S.Y. Schwartz, Directional site resonances and the influence of near-surface geology on ground motion, *Geophys. Res. Lett., 18(5)*, 901-904, 1991.

Boness, N. L., and M. D. Zoback, Stress-induced seismic velocity anisotropy and physical properties in the SAFOD Pilot Hole in Parkfield, CA, *Geophys. Res. Lett., 31*, L15S17, doi:10.1029/2003GL019020, 2004.

Brogna, A., S. La Delfa, V. La Monaca, S. Lo Nigro, D. Morelli, G. Patanè and G. Trincali, Measurements of indoor radon concrentation on the south-eastern flank of the Mount Etna volcano (Southern Italy), *J. Volcanol. Geotherm. Res., 165*, 71-75, 2007.

Burton, M., M. Neri, and D. Condorelli, High spatial resolution radon measurements reveal hidden active faults on Mt. Etna, *Geophys. Res. Lett., 31*, L07618, 2004.

Chouet, B. A., Excitation of a buried magmatic pipe: A seismic source model for volcanic tremor, *J. Geophys. Res., 90*, 1881-1893, 1985.

Chouet, B. A., Long-period volcano seismicity: its source and use in eruption forecasting, *Nature, 380*, 309-316, 1996.

Chouet, B., G. De Luca, G. Milana, P. Dawson, M. Martini and R. Scarpa, Shallow velocity of Stromboli volcano, Italy, derived from small-aperture array measurements of Strombolian tremor, *Bull. Seism. Soc. Am.,* 3, pp. 653–666, 1998.

Cochran, E. S., J. E. Vidale, and Y. G. Li, Near-fault anisotropy following the Hector Mine earthquake, *J. Geoph. Res., 108*, 2436, doi 10.1029/2002JB002352, 2003.

Cochran, E. S., Y. G. Li, and J. E. Vidale, Anisotropy in the shallow crust observed around the San Andreas Fault before and after the 2004 M 6.0 Parkfield earthquake, *Bull. Seism. Soc. Am., 96(4B)*, S364-S375, doi: 10.1785/0120050804, 2006.

Cultrera, G., A. Rovelli, G. Mele, R. M. Azzara, A. Caserta, and F. Marra, Azimuth-dependent amplification of weak and strong round motions within a fault zone (Nocera Umbra, central Italy), *J. Geoph. Res., 108(B3)*, 2156, doi:10.1029/2002JB001929, 2003.

Del Pezzo, E., S. De Martino, S. Gresta, M. Martini, G. Milana, D. Patanè, and C. Sabbarese, Velocity and spectral characteristics of the volcanic tremor at Etna deduced by a small seismometers array, *J. Volcanol. Geotherm. Res., 56*, 369-378, 1993.

Di Grazia, G., S. Falsaperla, and H. Langer, Volcanic tremor location during the 2004 Mount Etna lava effusion, *Geophys. Res. Lett., 33*, L04304, doi: 10.1029/2005GL025177, 2006.

Di Lieto, B., G. Saccorrotti, L. Zuccarello, M. La Rocca and R. Scarpa, Continuous tracking of volcanic tremor at Mount Etna, Italy, *Geophys. J. Int*., 169, 699-705, doi: 10.1111/j.1365-246X.2007.03316.x, 2007.

Ereditato, D., and G. Luongo, Volcanic tremor wavefield during quiescent and eruptive activity at Mt. Etna (Sicily), *J. Volcanol. Geotherm. Res., 61*, 239-251, 1994.

Falsaperla, S., S. Alparone, S. D’Amico, G. Di Grazia, F. Ferrari, H. Langer, T. Sgroi, and S. Spampanato, Volcanic tremor at Mt. Etna, Italy, preceding and accompanying the eruption of July-August, 2001, *Pure and Applied Geophys*., *162*, 2111-2132, doi: 10.1007/s00024-005-2719-y, 2005.

Faulkner, D. R., M. Mitchell, D. Healy, and M. J. Heap, Slip on weak faults by the rotation of regional stress in the fracture damage zone, *Nature, 444*, doi:10.1038/nature05353, 2006.

Fehler, M., Observations of volcanic tremor at Mount St. Helens Volcano, *J. Geophys. Res., 88*, 3476-3848, 1983.

Ferrucci, F., C. Godano, and N. A. Pino, Approach to the volcanic tremor by the covariance analysis: application to the 1989 eruption of Mt. Etna (Sicily), *Geophys. Res. Lett., 17*, 2425-2428, 1990.

Gresta, S., S. Imposa, D. Patanè and G. Patanè, Volcanic tremor at Mt. Etna: state-of-the-art and perspectives, *Pure Appl. Geophys., 125*, 255-271, 1987.

Immè, G., La Delfa, S. Lo Nigro, D. Morelli, and G. Patanè, Soil radon concentration and volcanic activity of Mt. Etna before and after the 2002 eruption, *Rad. Meas., 41*, 241-245, 2006a.

Immè, G., La Delfa, S. Lo Nigro, D. Morelli, and G. Patanè, Soil radon monitoring in NE flank of Mt. Etna (Sicily), *App. Rad. And Isot., 64*, 624-629, 2006b.

Jousset, P., and J. Douglas, Long-period earthquake ground displacements recorded on Guadeloupe (French Antilles), *Earthquake Engng. Struct. Dyn., 36(7)*, 949-964, 2007.

Jurkevics, A., Polarisation analysis of three-component array data, *Bull. Seismol. Soc. Am., 78*, 1725-1743, 1988.

Kanasewich, E.R., Time sequence analysis in Geophysics, *University of Alberta Press*, Edmonton, 1-532, 1981.

Konstantinous, I. K., and V. Schlindwein, Nature, wavefield properties and source mechanism of volcanic tremor: a review, *J. Volcanol. Geoterm. Res., 119*, 161-187, 2002.

Kvaerna, T., and F. Ringhdal, Stability of various f-k estimation techniques, Semiannual Technical Summary, *NORSAR Scientific Report*, 29-40, 1986.

La Rocca, M., D. Galluzzo, G. Saccorotti, S. Tinti, G. B. Cimini, and E. Del Pezzo E., Seismic signals associated with landslides and with a tsunami at Stromboli volcano, Italy. *Bull. Seism. Soc. Am., 94(5)*, 1850-1867, 2004.

Lentini, F., The geology of the Mt. Etna basement, *Mem. Soc. Geol. Ital., 23*, 7-25, 1982.

Lewis, M.A., Z. Peng, Y. Ben-Zion, and F. L. Vernon, Shallow seismic trapping structure in the San Jacinto fault zone near Anza, California, *Geophys. J. Int., 162*, 867-881, 2005.

Li, Y.G. and P. C. Leary, Fault zone trapped seismic waves, *Bull. Seism. Soc. Am., 80*, 1245-1271, 1990.

Louie, N.J., Faster, better shear-wave velocity to 100 meters depth from refraction microtremor arrays, *Bull. Seism. Soc. Am., 91*, 347-364, 2001.

Metaxian, J.P., P. Lesage, and J. Dorel, Permanent tremor of Masaya volcano, Nicaragua: wave field analysis and source location, *J. Geophys. Res., 102*, 22529-22545, 1997.

Milana, G., A. Rovelli, A. De Sortis, G. Calderoni, G. Coco, M. Corrao, and P. Marsan, The role of long-period ground motions on magnitude and damage of volcanic earthquakes on Mt. Etna, Italy, *Bull. Seism. Soc. Am., 98*(6), 2724–2738, doi: 10.1785/0120080072, 2008.

Morelli, D., G. Immè, S. La Delfa, S. Lo Nigro, and G. Patanè, Evidence of soil radon as tracer of magma uprising at Mt. Etna, *Rad. Meas., 41*, 721-725, 2006.

Neri, M., V. Acocella, and B. Behncke, The role of the Pernicana Fault System in the spreading of Mt. Etna (Italy) during the 2002-2002 eruption, *Bull. Volcanol., 66*, 417-430, doi:10.1007/S00445-003-0322-X, 2004.

Obrizzo, F., F. Pingue, C. Troise, and G. De Natale, Coseismic displacements and creeping along the Pernicana fault (Etna, Italy) in the last 17 years: a detailed study of a tectonic structure on a volcano, *J. Volcanol. Geotherm. Res., 109*, 109-131, 2001.

Park, C. B., R. D. Miller, and J. Xia, Multi-channel analysis of surface waves (MASW), *Geophysics, 64*, 800-808, 1999.

Privitera, E., T. Sgroi, and S. Gresta, Statistical analysis of intermittent volcanic tremor associated with the September 1989 summit explosive eruptions at Mt. Etna, Sicily, *J. Volcanol. Geotherm. Res., 120*, 235-247, 2003.

Puglisi, G., and V. Acocella, Integrated study to define the hazard of the instable flanks of Etna: the DPC-INGV 2008-2010 project, *EGU 2008 General Assembly, Session "Volcano Flank Instability"*, A-06863, 2008.

Richwalski, S. M., M. Picozzi, S. Parolai, C. Milkereit, F. Baliva, D. Albarello, K. Roy-Chowdhury, H. van der Meer and J. Zschau, Rayleigh wave dispersion curves from seismological and engineering-geotechnical methods: a comparison at the Bornheim test site (Germany), *J. Geophys. Eng.*, *4*, 349-361, doi:10.1088/1742-2132/4/4/001, 2007.

Rigano, R., F. Cara, G. Lombardo, and A. Rovelli, Evidence for ground motion polarization on fault zones of Mount Etna volcano, *J. Geophys. Res., 113*, B10306, doi:10.1029/2007JB005574, 2008.

Ripepe, M., M. Coltelli, E. Privitera, S. Gresta, M. Moretti, and D. Piccinini, Seismic and infrasonic evidences fora n impulsive source of the shallow volcanic tremor at Mt. Etna, Italy, *Geophys. Res. Lett., 28*, 1701-1704, 2001.

Rovelli, A., A. Caserta, F. Marra, and V. Ruggiero, Can seismic waves be trapped inside an inactive fault zone? The case study of Nocera Umbra, central Italy, *Bull. Seismol. Soc. Am., 92*, 2217-2232, 2002.

Rust, D., B. Behncke, M. Neri, and A. Ciocanel, Nested zones of instability in the Mount Etna volcano edifice, Italy, *J. Volcanol. Geotherm. Res., 144*, 137-153, 2005.

Saccorotti, G., L. Zuccarello, E. Del Pezzo, J. Ibanez, and S. Gresta, Quantitative analysis of the tremor wavefield at Etna Volcano, Italy, *J. Volcanol. Geotherm. Res., 136*, 223-245, 2004.

Sambridge, M., Geophysical inversion with a neighbourhood algorithm I. Searching a parameter space, *J. Geophys. Res., 103*, 4839-4878, 1999.

Schubnel, A., and Y. Guéguen, Dispersion and anisotropy of elastic waves in cracked rocks, *J. Geophys. Res., 108(B2)*, 2101, doi:10.1029/2002JB001824, 2003.

Seidl, D., R. Schick and M. Riuscetti, Volcanic tremors at Etna: a model for hydraulic origin, *Bull. Volcan., 44 (1)*, 43-56, 1981.

Spudich, P., M. Hellweg, and H. K. Lee, Directional topographic site response at Tarzana observed in aftershocks of the 1994 Northridge, California, earthquake: implications for mainshock motions, *Bull. Seism. Soc. Am., 86*, S193-S208, 1996.

Tibaldi, A., and G. Groppelli, Volcano-tectonic activity along structures of the unstable NE flank of the Mt. Etna (Italy) and their possible origin, *J. Volcanol. Geotherm. Res., 115*, 277-302, 2002.

Tokimatsu, K., Geotechnical site characterization using surface waves, in Earthquake Geotechnical Engineering, K. Ishihara (Editor), Balkema, Rotterdam, 1333-1368, 1997.

Wathelet, M., D. Jongmans, M. Ohrnberger and S. Bonnefoy-Claudet, Array performances for ambient vibrations on a shallow structure and consequences over vs inversion, *J. Seismol., 12*, 1-19, doi:10.1007/s10950-007-9067-x, 2008.

Wathelet, M., Array recordings of ambient vibrations: surface waves inversion, *Ph. D. Thesis*, University of Liege, Belgium, 177 pp., 2005.

Wegler, U., and D. Seidl, Kinematic parameters of the tremor wavefield at Mt. Etna (Sicily), *Geophys. Res. Lett., 24*, 759-762, 1997.

Wu, J., J. A. Hole, J. A. Snoke and M. G. Imhof, Depth extent of the fault-zone seismic waveguide: effects of increasing velocity with depth, *Geophys. J. Int., 173*, 611-622, doi:10.1111/j.1365-246X.2008.03755.x, 2008.

Figure Captions

Figure 1 Top) Geology of Mt. Etna, redrawn from Acocella and Neri (2005). Bottom) Detailed map of the *PFS*, colour is proportional to topography (from blue to red). The black rectangle indicates the area where we concentrated the ambient noise measurements (*Piano Pernicana*). SUM, NEC and SEC indicate Summit Craters area, northeast Crater, and southeast Crater, respectively, where different authors localize the source of volcanic tremor during the recent eruptions.

Figure 2 Top) Map of Mt. Etna. The grey lines indicate the NE Rift and the *PFS,* and the filled black circles with numbers indicate the sites where temporary (about 30 min) tremor measurements were performed (see also Table 1).
Bottom) Detail of the *Piano Pernicana* area (dashed rectangle of the top panel) with the location of measurement sites. The white cross symbol shows the array location. Full lines provide topography variations.

Figure 3 Example of shot recordings using forty eight 4.5-Hz vertical geophones (unfilled triangles) with regular spacing of 2 m. The shot offset is -20 m from the first geophone. We have plotted the first 2 s of the signals. The black triangles over the linear array indicate the positions of the shots using a mini-bang source.

Figure 4 Geometry of the 2D array equipped with long-period seismometers (LE3D/5 s, with eigenfrequency of 0.2 Hz). The location of the array experiment is indicated in the bottom panel of Figure 2 by a white cross symbol. The filled black triangles indicate sensors without a locked GPS signal during the experiment. The unfilled triangles show the sensors used in the array analysis. The H/V spectral ratios of stations s1, s2, s3 and s4 are shown in Fig. 8.

Figure 5 Noise recordings and Fourier amplitude spectra of the three components of representative measurements. Top) The location of measurement site #30 is close to the crater area (see Fig. 2); Middle and Bottom) The location of measurement sites #5 and #10 is at *Piano Pernicana*, see details in Fig. 6. The spectra of EW, NS and Z components are plotted in black, grey and dotted lines, respectively (counts in the amplitude scale).

Figure 6 The filled black circles with numbers indicate the location of measurement sites of seismic noise in the area around the array. The location of the 2D array is indicated by a cross and the thick grey line shows the trace position of the fault.

HVSR and polarization results are shown for measurement sites #3, #4, #5, #6, #7, #9, #10, #11, #12, #13 (red circles) and one station of the 2D array.
The contouring plots show the geometric mean of horizontal-to-vertical spectral ratios (HVSR) as a function of frequency (x-axis) and direction of motion (y-axis) for tremor recordings. The contours of HVSRs are plotted up to 4 Hz and the maximum value of amplitude scale is 10. At sites #5 and #10 the individual curves for each rotated horizontal-to-vertical spectral ratio are also shown. The rose diagrams indicate the results from polarization analysis. Note the variation of polarization crossing the main trace of the *PFS* (indicated as thick grey line). Measurement sites #3, #4, #5 and #6 show a polarization of about 120° (clockwise from north), the remaining measurements show a polarization of about 160°.

Figure 7 Histograms of polarization angles computed over running time-windows throughout tremor records, at representative measurement sites north and south of the fault trace (see Fig. 6).

Figure 8 Top) HVSR of four selected stations (s1,s2,s3, and s4) of the 2D array (see also Fig. 4). Bottom) HVSRs are plotted for the 160° rotated motions at the 16 stations of the 2D array. We also report the location map with a detail of the distance between the array site and measurement site #5.

Figure 9 HVSR at measurement site #5 (the camping ground *Clan Ragazzi,* about 300 m from the array site; see the previous figure) computed at different times.

Figure 10 Particle motion along two transects crossing the fault. Five minutes of volcanic tremor are band-pass filtered between 0.5 and 2 Hz where we observe the largest directional effect. For each transect, the panel on the left hand shows the particle motion in the horizontal plane (n-e). After the rotation to the direction of maximum polarization, the particle motion is plotted in the vertical plane (panel on the right hand, z-rad). The label array indicates one station of the 2D array.

Figure 11 HVSR and polarization results of measurements carried out in April 2008 (red circles; see also Table 1) at *Piano Pernicana*. Note the variation of polarization crossing the main trace of fault (indicated as a thick grey line). Measurements #16, #17, #18 and #19 were performed in the same area of the *PFS* shown in Fig. 6. The remaining measurements (from #20 to #28) were performed approximately in a transect 900 m to the east.

Figure 12 HVSR and polarization results of measurements far from the array area (indicated by the dashed rectangle). Measurement sites #29, #30 and # 31 are near the NE Rift (Table 1). The thick grey lines indicate the NE Rift and the *PFS*. For the sake of comparison, the direction of fast velocity found by *Bianco et al*. [2007] using shear-wave splitting analysis is also shown (thick black arrows) for seismic stations used in their analysis (filled black triangles; DMT, NOC, CCV, B92, MNT, ESP, POM).

Figure 13 Top) Example of slowness-frequency map obtained for the shot of Figure 3 after the *f-k* analysis. The black curve within 10-20 Hz shows the picked dispersion curve. Middle) Average dispersion curve estimated using vertical components. The dispersion curve in the 2-5 and 7-35 Hz frequency bands was computed using the 2D array of seismological sensors and the two linear arrays of geophones, respectively. In the former frequency band (2-5 Hz) we performed *f-k* analysis over tremor data, in the latter frequency band (7-35 Hz) we use active sources (mini-gun shots). Bottom) Back-azimuth inferred through *f-k* analysis of tremor data recorded at the 2D array.

Figure 14 Top) Theoretical dispersion curves for models obtained from the inversion overlaid by the observed phase-velocity (filled circles) for the vertical component. Gray tonality is proportional to the misfit computed in the inversion. Middle) 1-D layered Vs profiles obtained by inverting the dispersion curves. Bottom) Theoretical 1D transfer functions (SH case) computed for all models in the middle panel.

Figure 15 Earthquake data analysis at site #5 (the camping ground *Clan Ragazzi*). a) Three components of ground motion of seismograms of Table 2. b) Horizontal polarization of the seismograms computed on moving time windows of 2 sec. The rose diagrams in the inset indicate the mean polarization computed on the entire seismogram. c) Rectilinearity computed on moving time windows. d) Azimuthal pattern of H/V spectral ratios. Note the consistency of the directional effect using different earthquakes i) between the main directions of the rose diagrams and the azimuthal pattern of H/V spectral ratios, and, ii) between earthquake and tremor data analyses (see also Figs. 6 and 9).

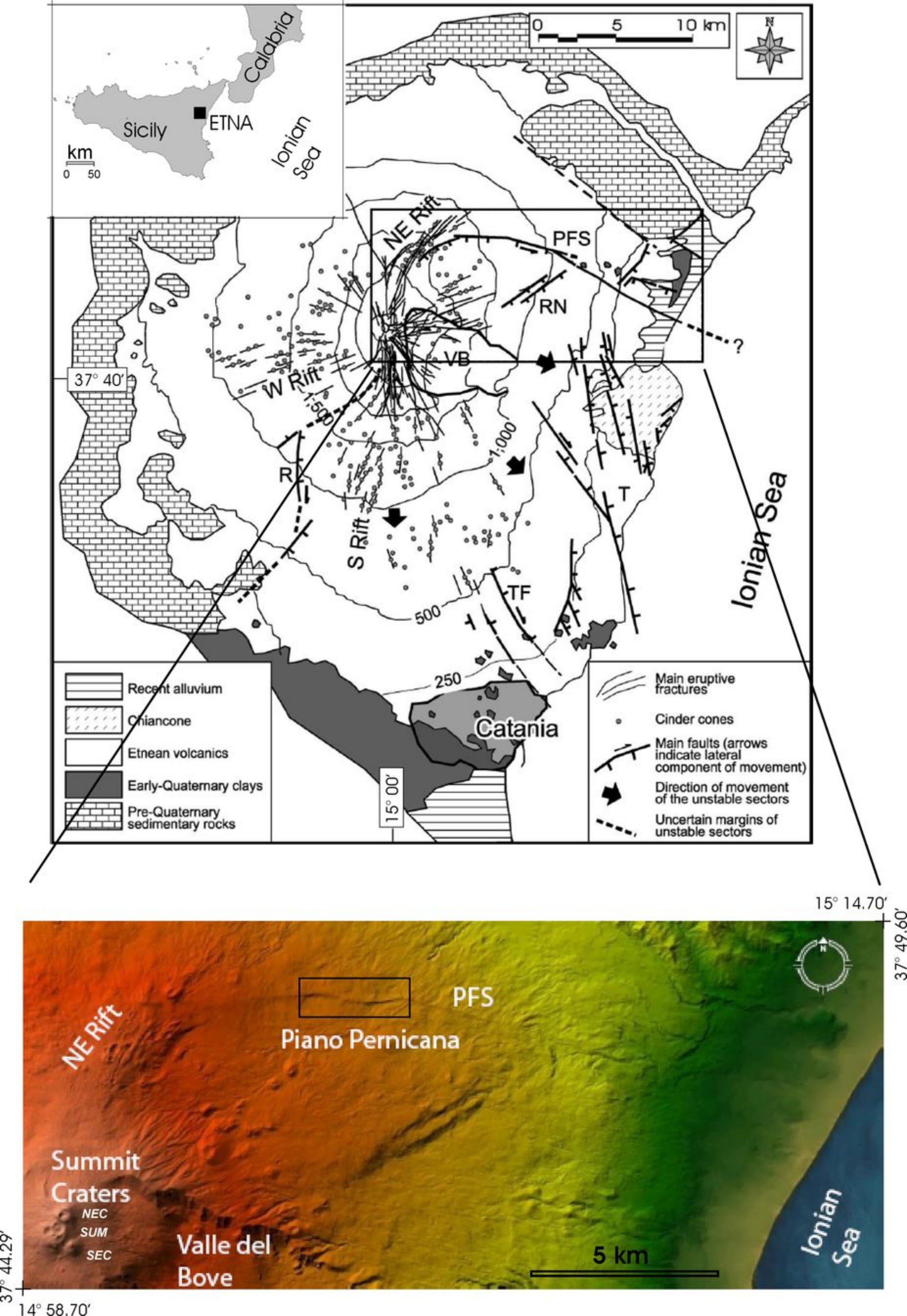
Calabria
Sicily
ETNA
Ionian Sea
km
0 50
0 5 10 km
N
NE Rift
PFS
RN
VB
W Rift
1,500
1,000
500
250
R
S Rift
T
TF
?
37° 40′
15° 00′
Catania
Ionian Sea
Recent alluvium
Chiancone
Etnean volcanics
Early-Quaternary clays
Pre-Quaternary sedimentary rocks
Main eruptive fractures
Cinder cones
Main faults (arrows indicate lateral component of movement)
Direction of movement of the unstable sectors
Uncertain margins of unstable sectors
15° 14.70′
37° 49.60′
NE Rift
PFS
Piano Pernicana
Summit Craters
NEC
SUM
SEC
Valle del Bove
5 km
Ionian Sea
37° 44.29′
14° 58.70′

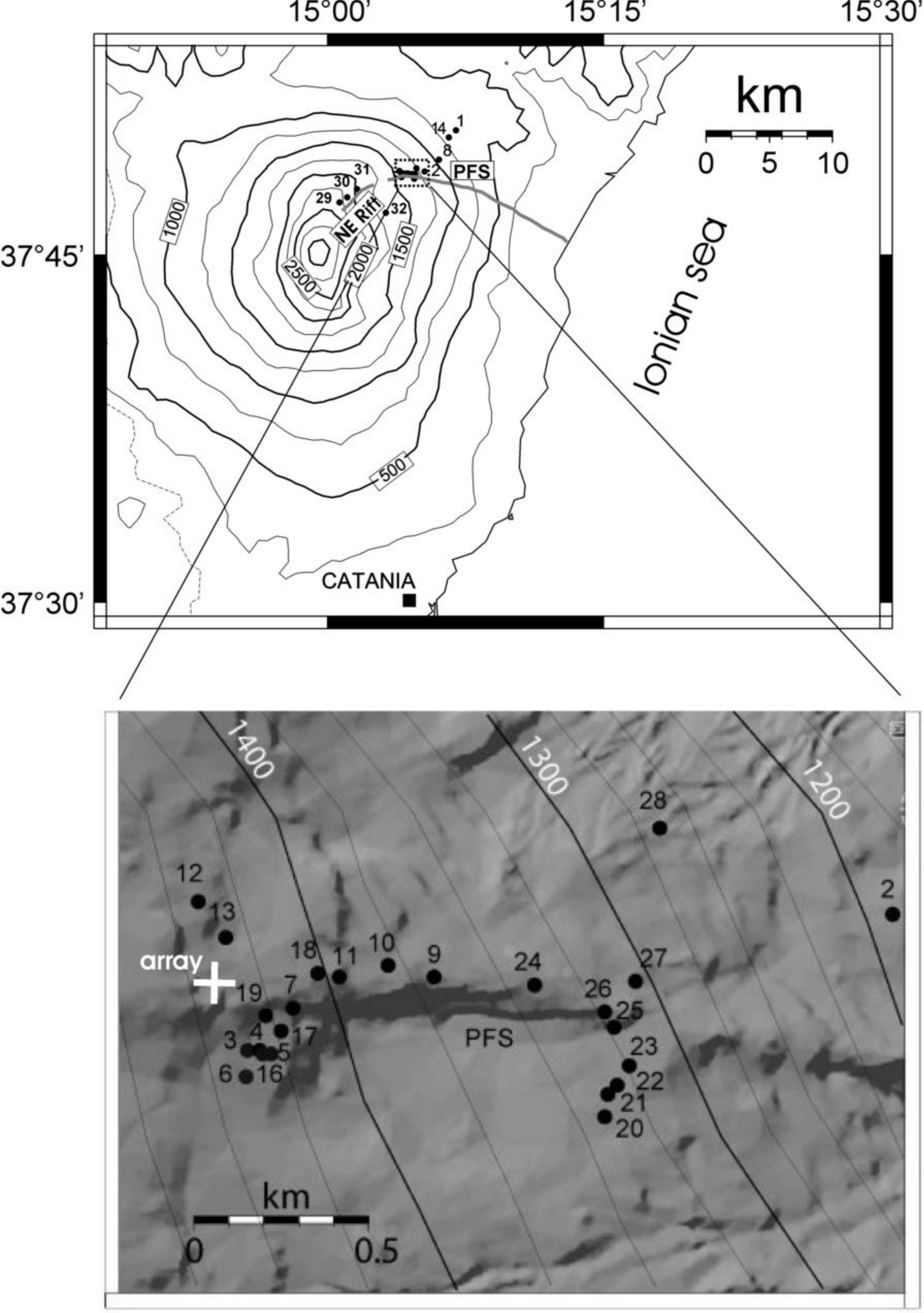
15°00'
15°15'
15°30'
37°45'
37°30'
km
0 5 10
Ionian sea
CATANIA
PFS
NE Rift
1000
1500
2000
2500
500
1
14
8
2
29
30
31
32
1400
1300
1200
28
12
13
2
array
18
11
10
9
24
27
26
25
19
7
17
3
4
5
6
16
PFS
23
22
21
20
km
0 0.5

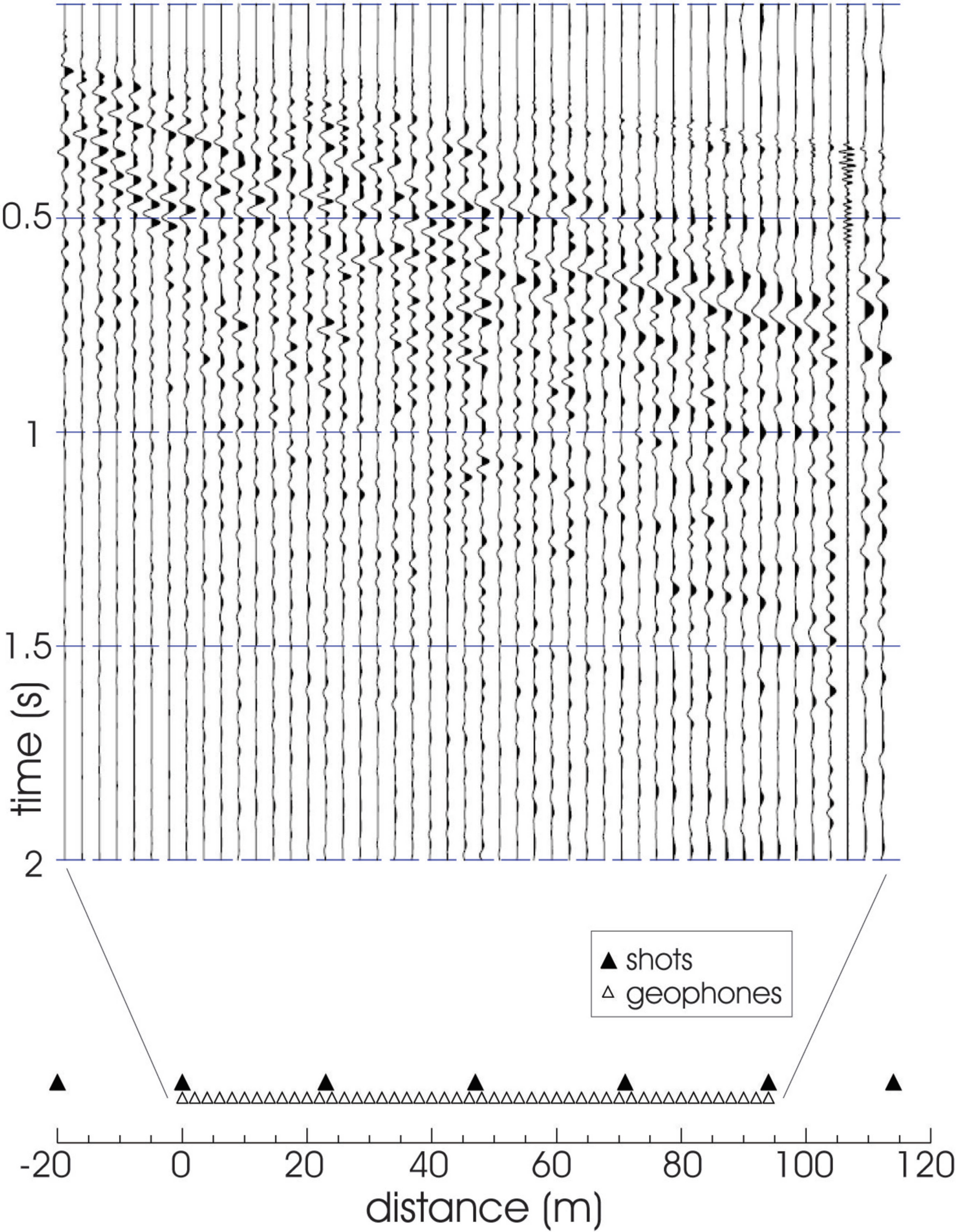
0.5
1
1.5
2
time (s)
shots
geophones
-20
0
20
40
60
80
100
120
distance (m)

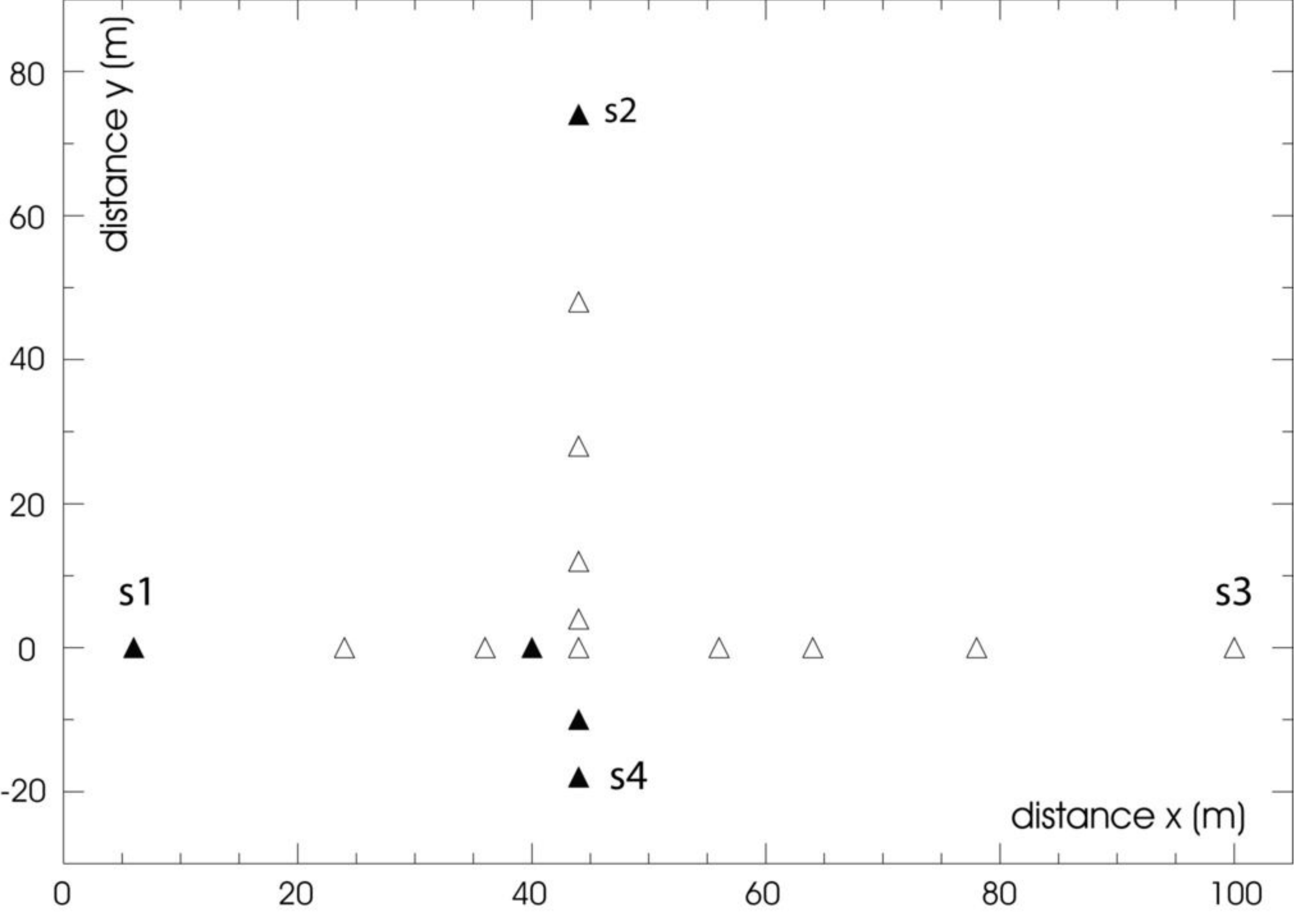

distance y (m)
80
60
40
20
0
-20
s2
s1
s3
s4
distance x (m)
0
20
40
60
80
100

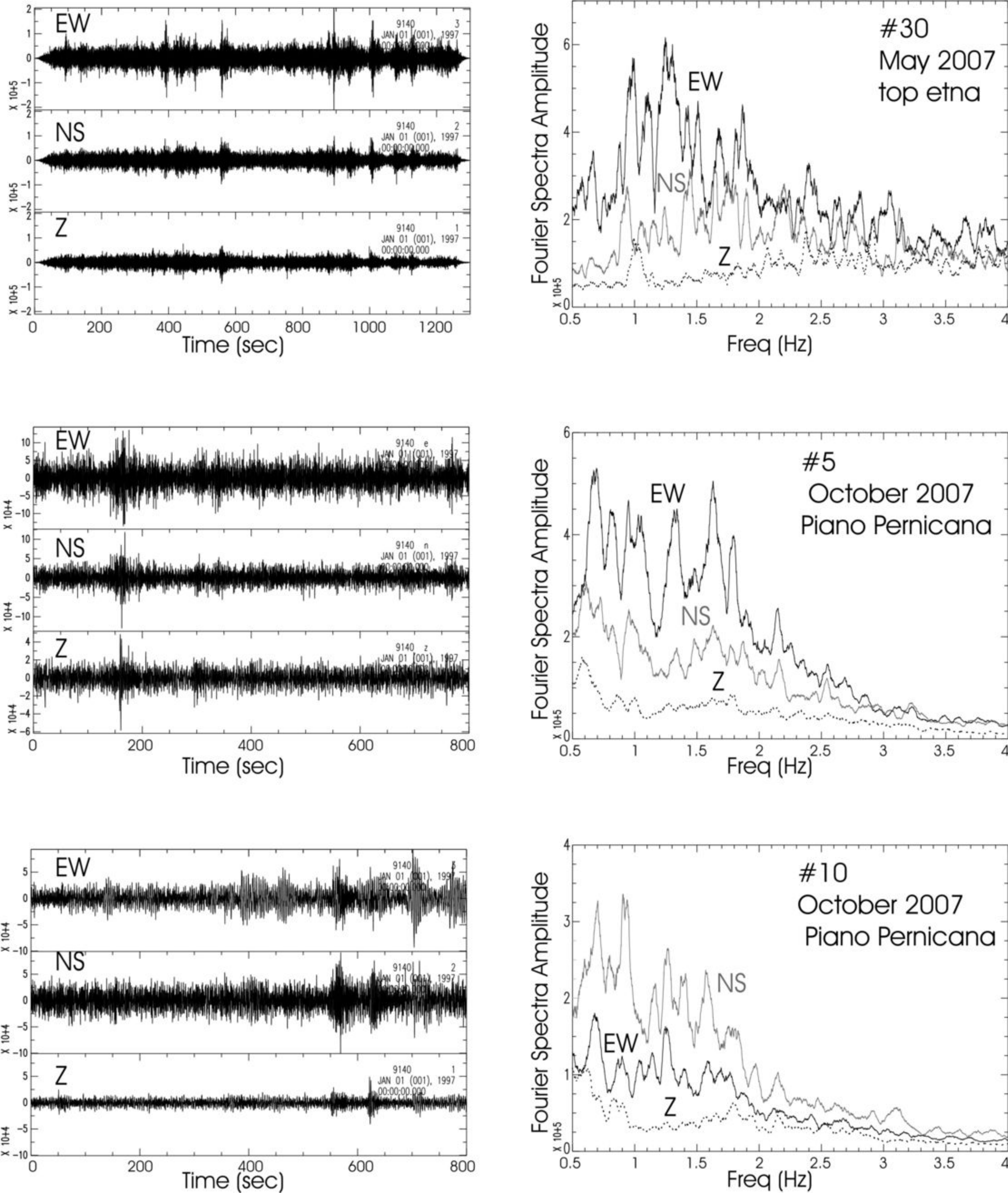
EW
NS
Z
9140 3
JAN 01 (001), 1997
00:00:00.000
X 10+5
Time (sec)
Fourier Spectra Amplitude
Freq (Hz)
#30
May 2007
top etna
EW
NS
Z
X 10+4
#5
October 2007
Piano Pernicana
#10
October 2007
Piano Pernicana

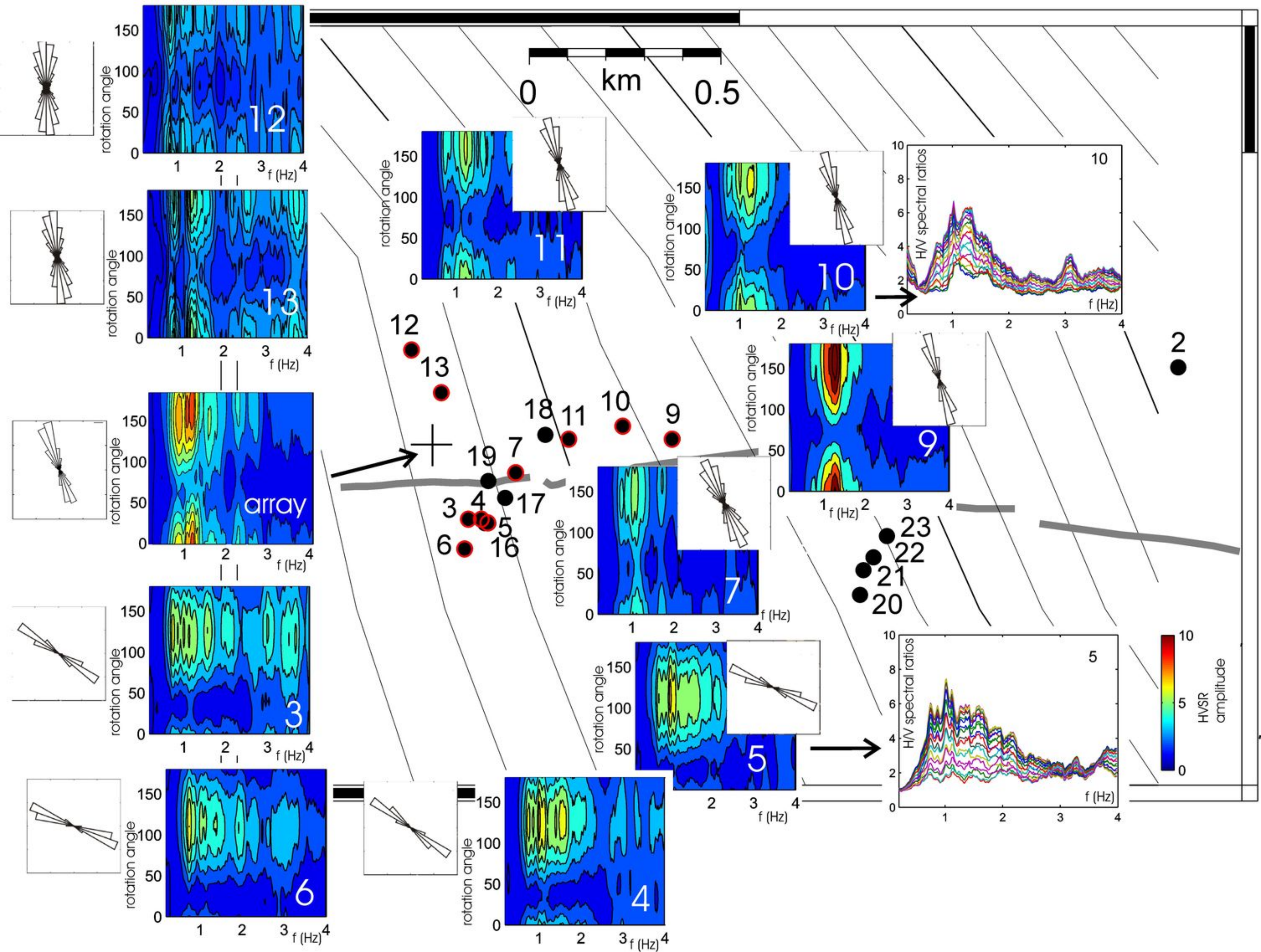

0
km
0.5
12
13
array
3
6
11
10
9
7
5
4
rotation angle
f (Hz)
H/V spectral ratios
HVSR amplitude
2
18
19
16
17
20
21
22
23

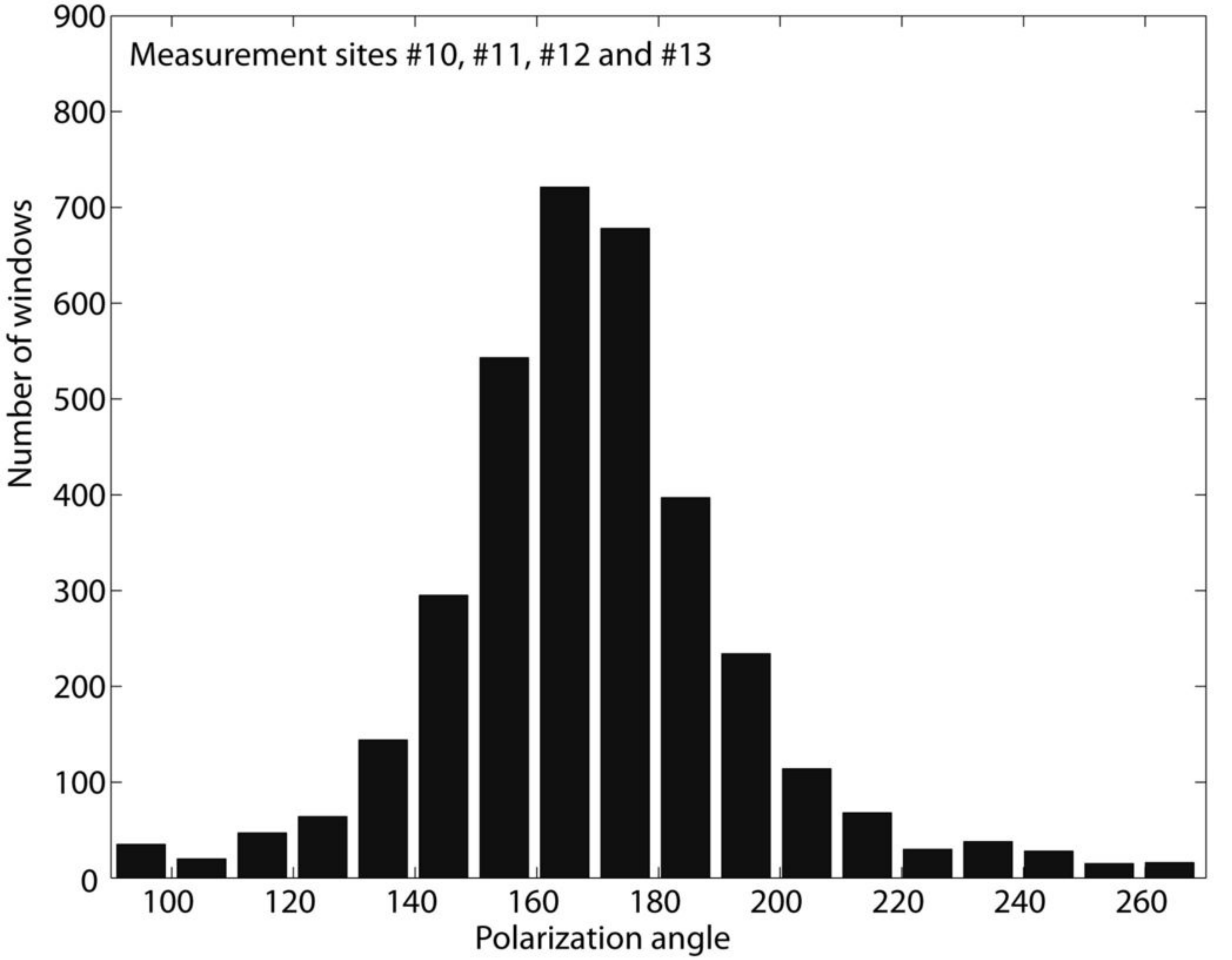
Measurement sites #10, #11, #12 and #13
Number of windows
Polarization angle
0
100
200
300
400
500
600
700
800
900
100
120
140
160
180
200
220
240
260

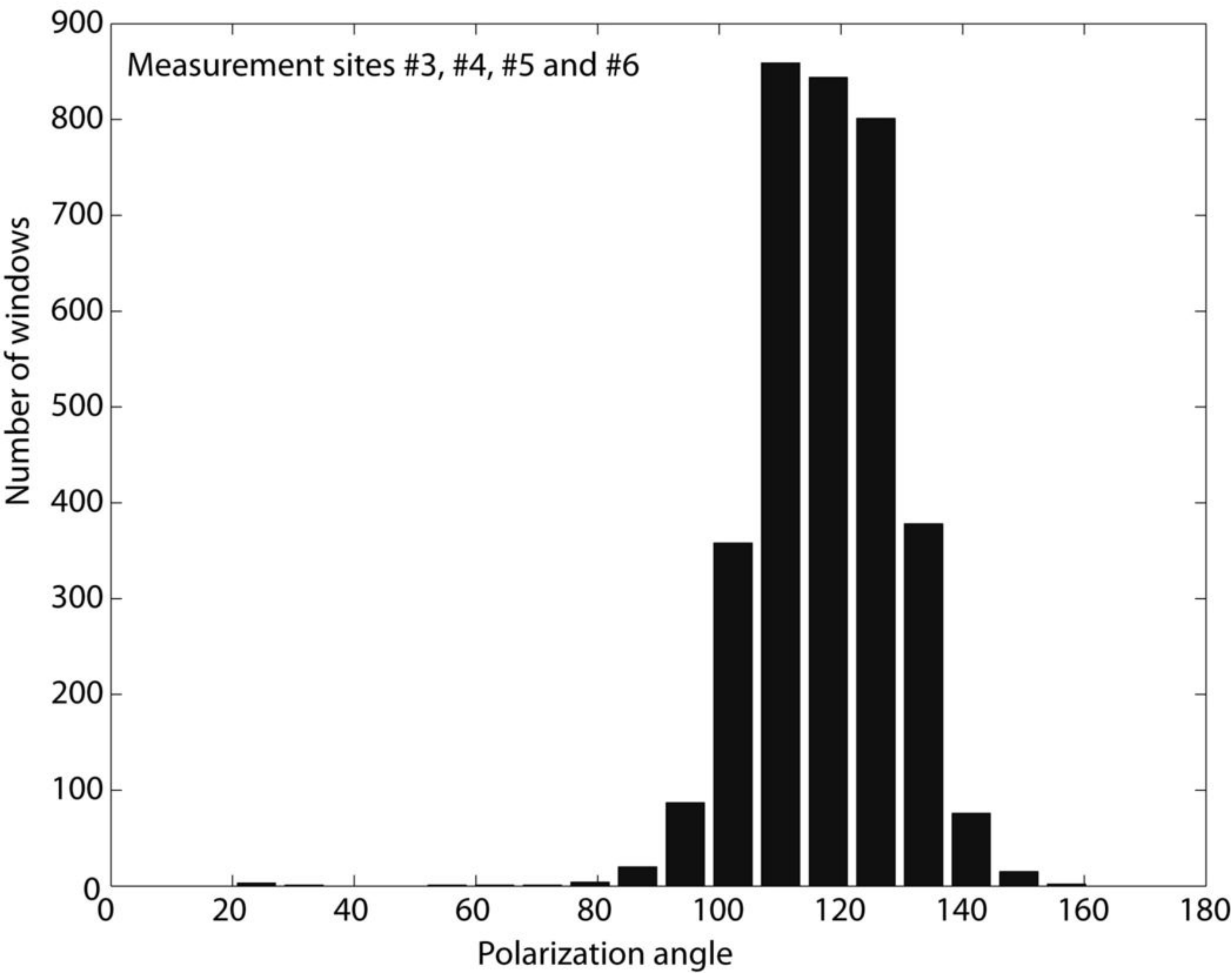
Measurement sites #3, #4, #5 and #6
Number of windows
Polarization angle
0
100
200
300
400
500
600
700
800
900
0
20
40
60
80
100
120
140
160
180

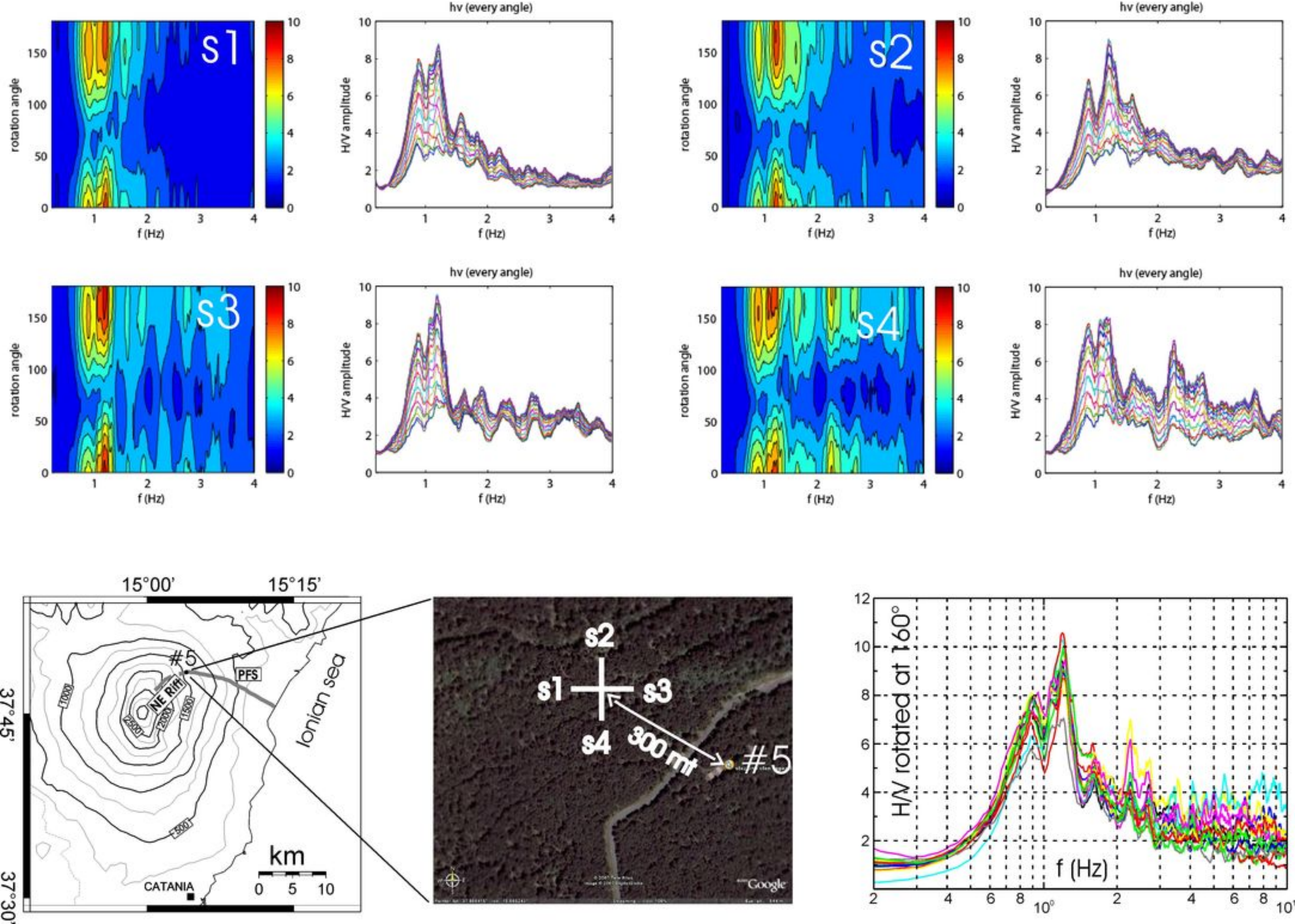
s1
s2
s3
s4
hv (every angle)
rotation angle
H/V amplitude
f (Hz)
15°00'
15°15'
37°45'
37°30'
#5
PFS
NE Rift
Ionian sea
1000
1500
2000
2500
500
km
0 5 10
CATANIA
300 mt
Google
H/V rotated at 160°

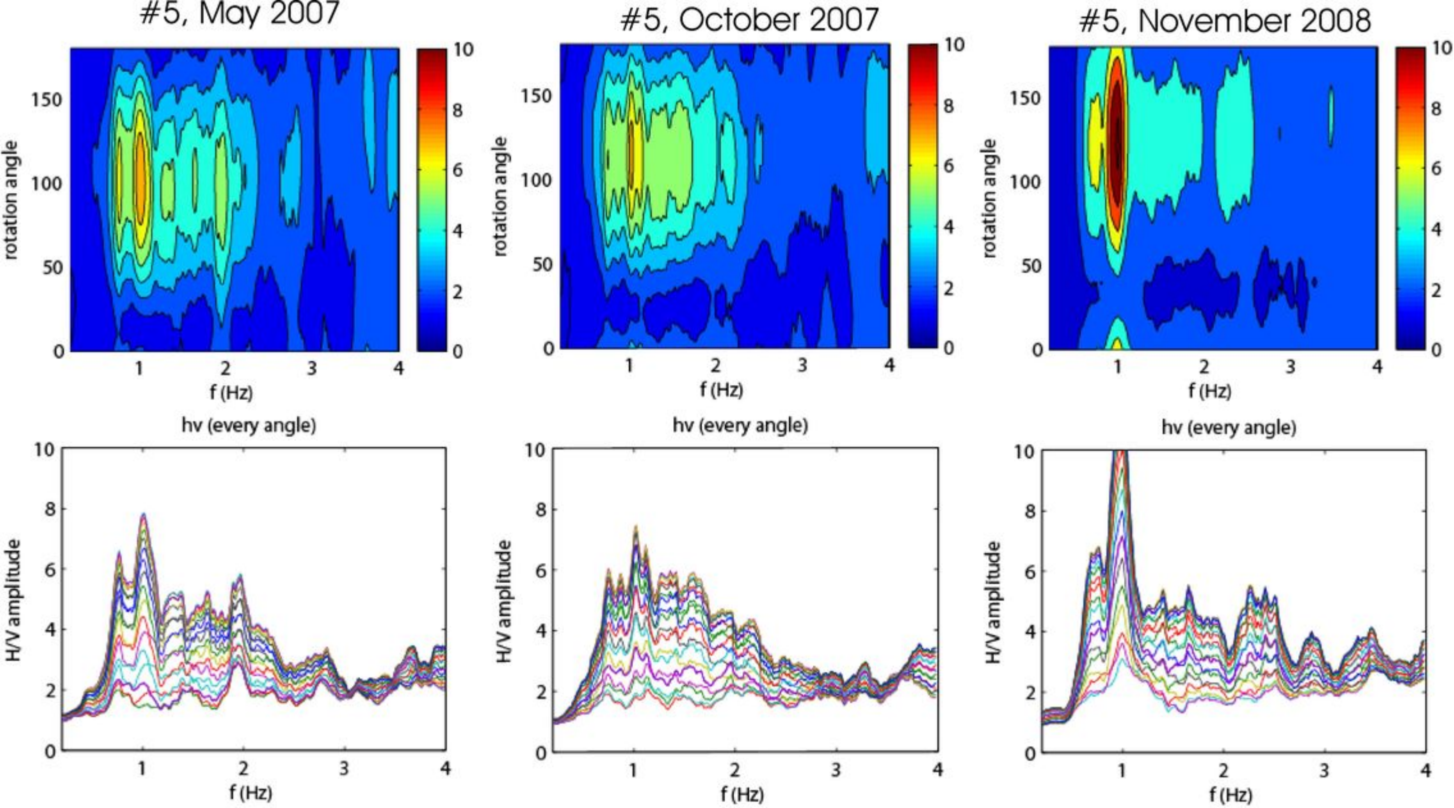

#5, May 2007
#5, October 2007
#5, November 2008
rotation angle
f (Hz)
hv (every angle)
H/V amplitude


a)
Western Transect
Plane n-e
Plane z-rad
n
e
z
rad
#12
#13
#11
array
#7
#3
#5
#6
b)
Eastern Transect
Plane n-e
Plane z-rad
#28
#27
#26
#25
#23
#22
#21
#20

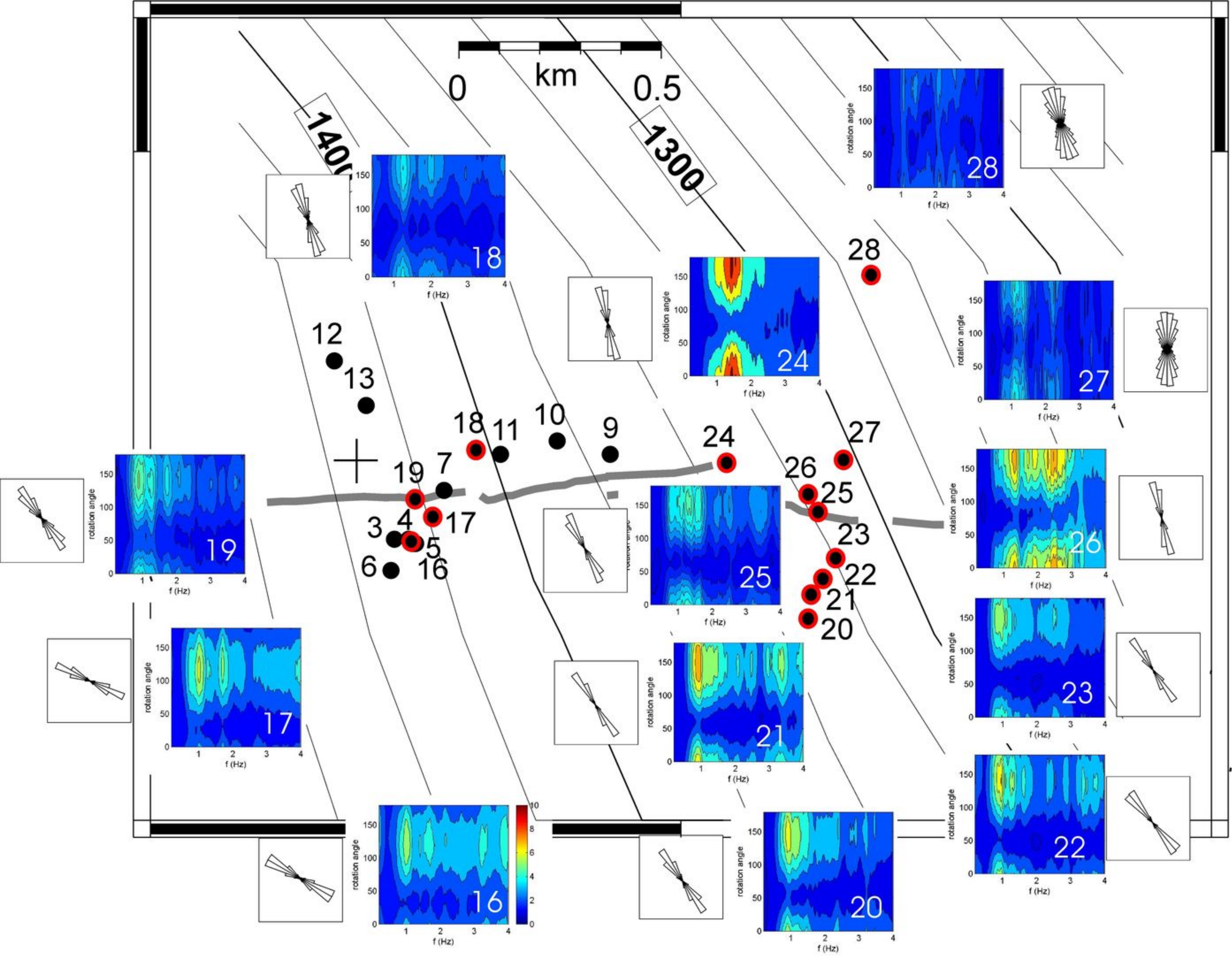

0
km
0.5
1400
1300
12
13
18
11
10
9
24
28
27
26
25
19
7
17
3
4
5
6
16
23
22
21
20
rotation angle
f (Hz)

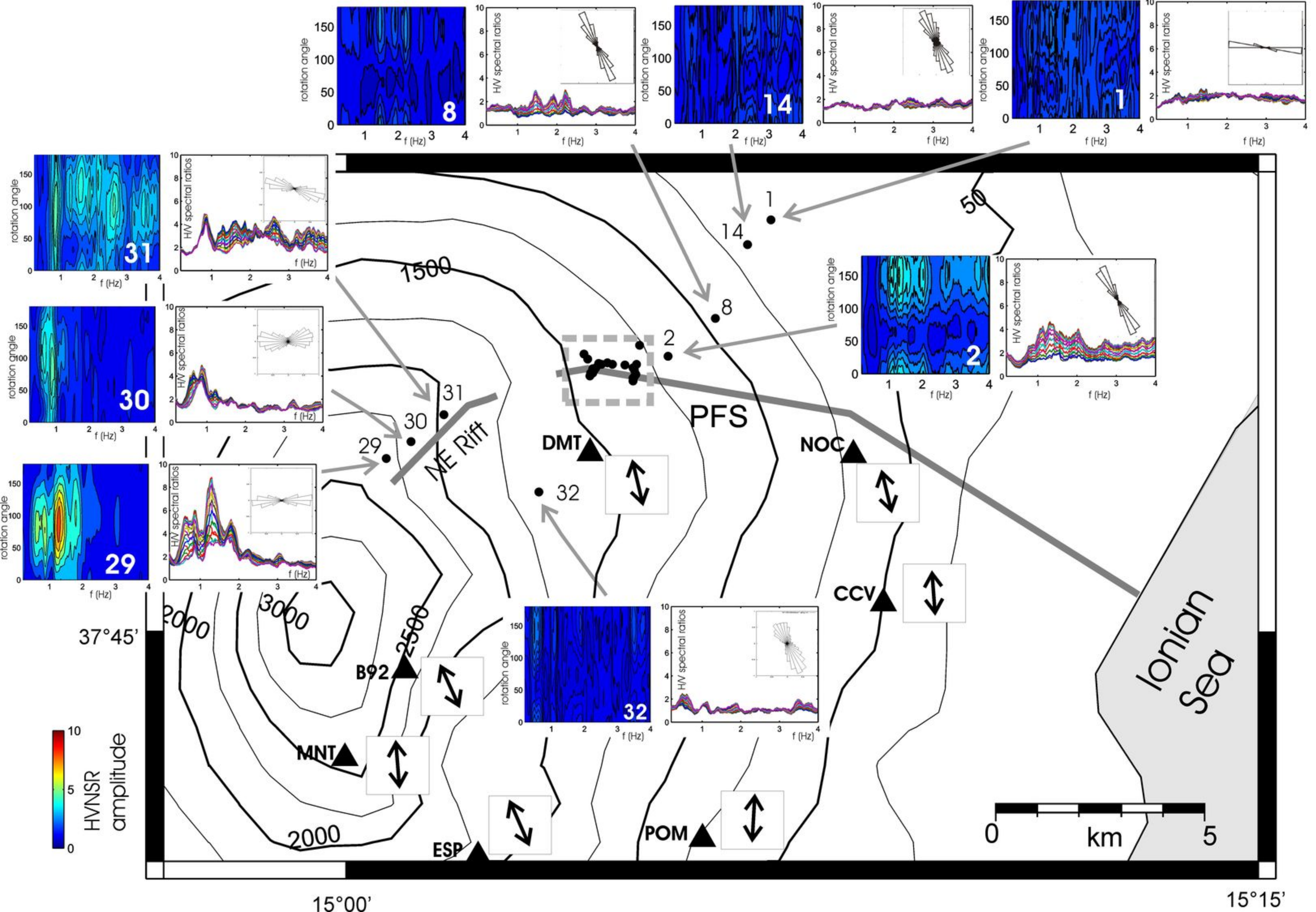

rotation angle
H/V spectral ratios
f (Hz)
8
14
1
31
30
29
2
32
1500
2000
2500
3000
50
PFS
NE Rift
DMT
NOC
CCV
B92
MNT
ESP
POM
Ionian Sea
HVNSR amplitude
0
km
5
37°45'
15°00'
15°15'

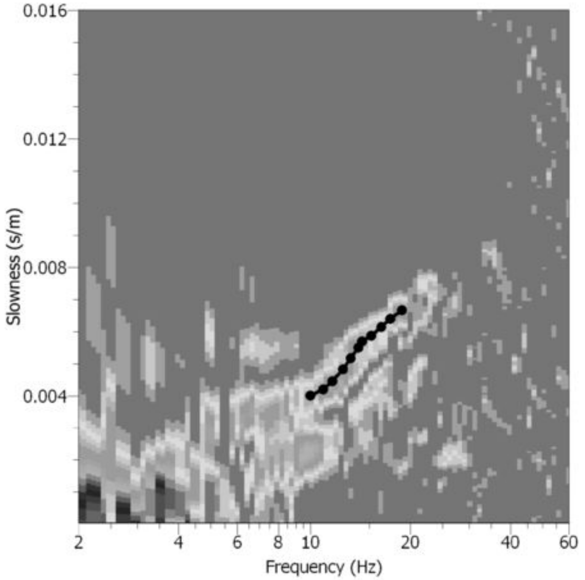
0.016
0.012
0.008
0.004
Slowness (s/m)
2
4
6
8
10
20
40
60
Frequency (Hz)

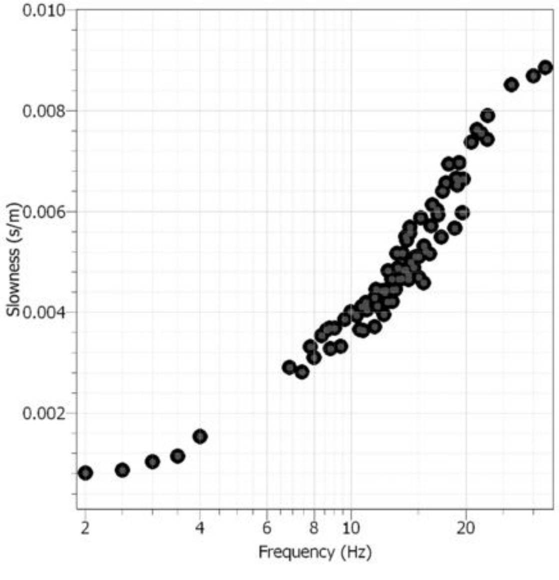
0.010
0.008
0.006
0.004
0.002
Slowness (s/m)
2
4
6
8
10
20
Frequency (Hz)

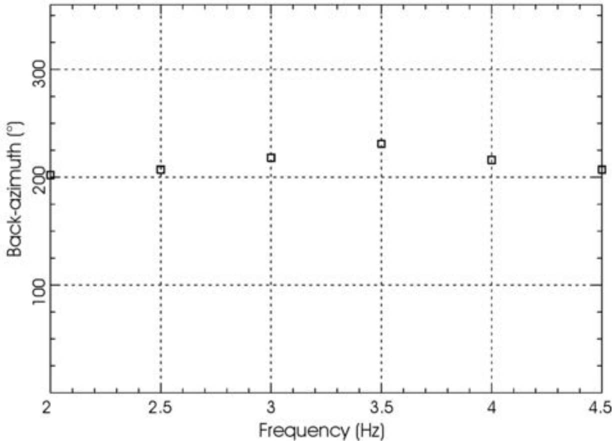
300
200
100
Back-azimuth (°)
2
2.5
3
3.5
4
4.5
Frequency (Hz)

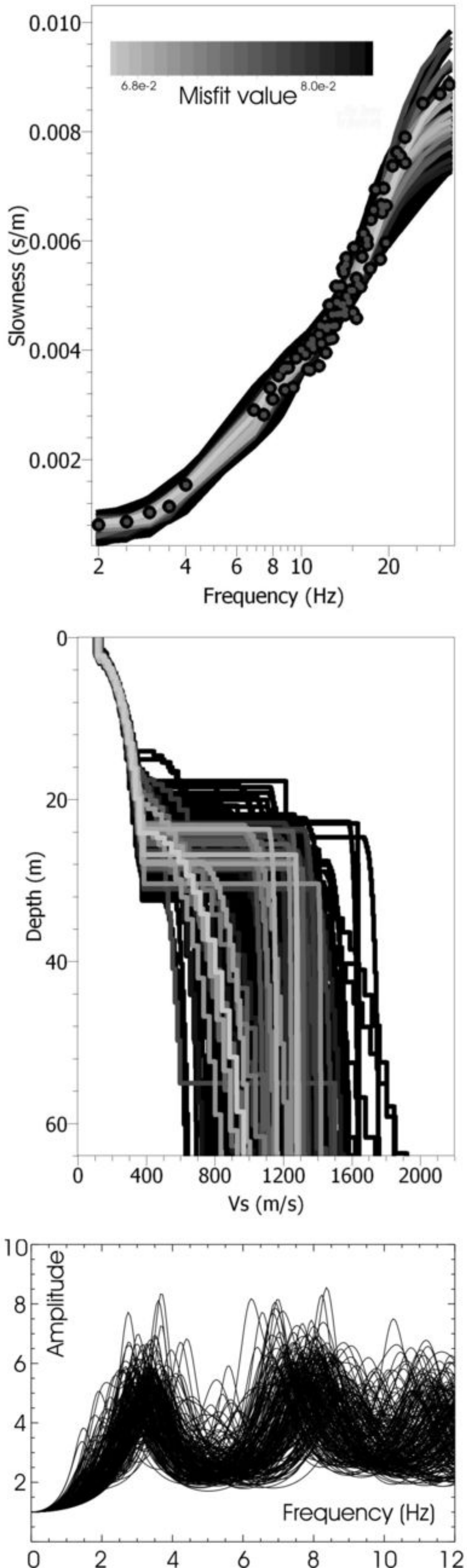

Misfit value
6.8e-2
8.0e-2
Slowness (s/m)
0.010
0.008
0.006
0.004
0.002
2
4
6
8
10
20
Frequency (Hz)
Depth (m)
0
20
40
60
0
400
800
1200
1600
2000
Vs (m/s)
Amplitude
Frequency (Hz)
10
8
6
4
2
0
2
4
6
8
10
12

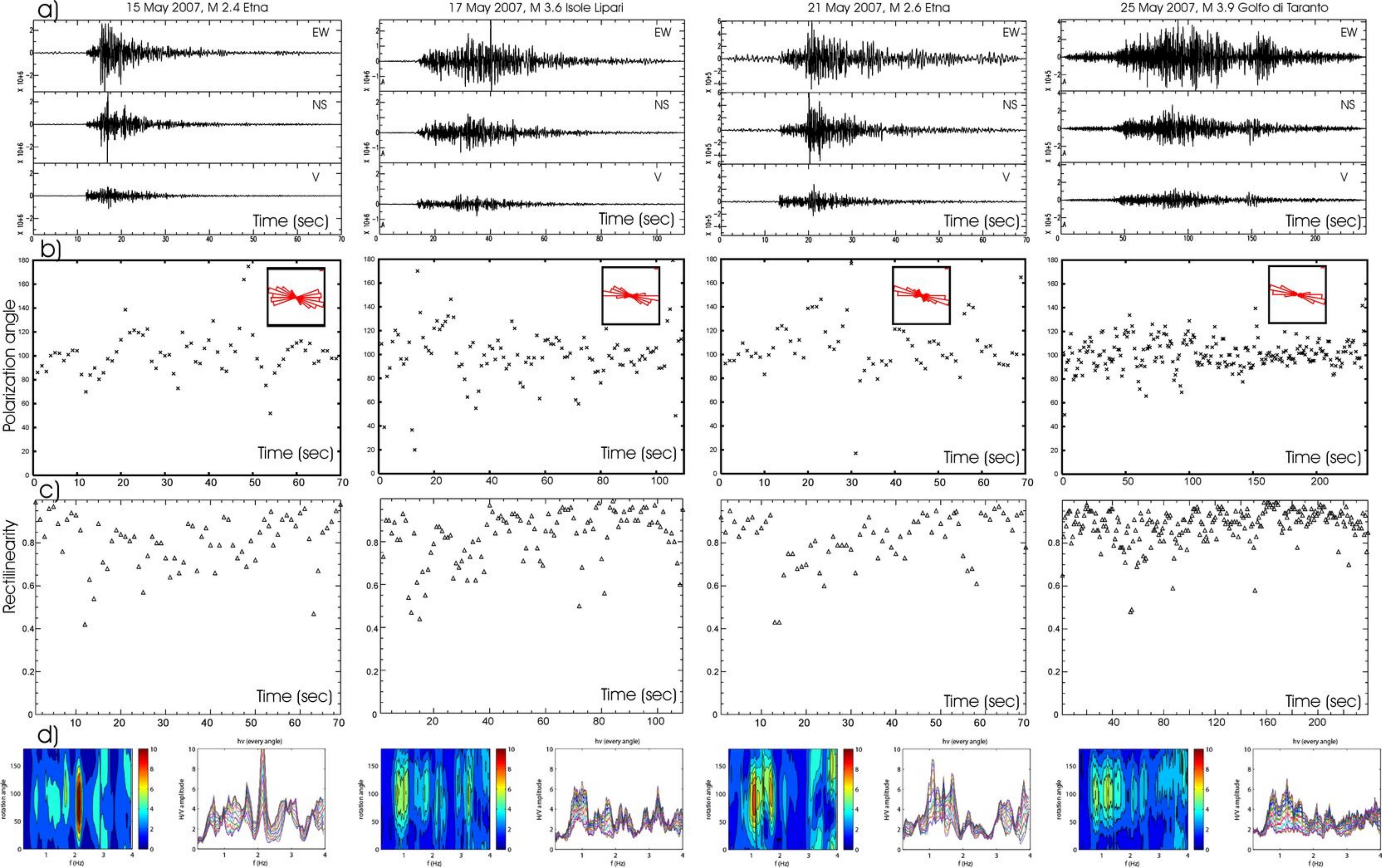

a)
15 May 2007, M 2.4 Etna
17 May 2007, M 3.6 Isole Lipari
21 May 2007, M 2.6 Etna
25 May 2007, M 3.9 Golfo di Taranto
EW
NS
V
Time (sec)
b)
Polarization angle
c)
Rectilinearity
d)
rotation angle
f (Hz)
hv (every angle)
H/V amplitude